

Assessment of Thermo-Hydraulic Performance of MXene Based Nanofluid as Coolant in a Dimpled Channel: A Numerical Approach

F. Ahmed^{a,*}, Achiya Khanam^b, L. Samylingam^c, Navid Aslfattahi^d, R. Saidur^{c,e}

^aInstitute of Nuclear Power Engineering, Bangladesh University of Engineering and Technology, Dhaka, 1000, Bangladesh

^bDepartment of Coatings and Polymeric Materials, North Dakota State University, Fargo, USA

^cResearch Center for Nano-Materials and Energy Technology (RCNMET), School of Engineering and Technology, Sunway University, Bandar Sunway, Petaling Jaya, 47500, Selangor Darul Ehsan, Malaysia

^dDepartment of Fluid Mechanics and Thermodynamics, Czech Technical University, Technica 4, 160 00, Prague, Czech Republic.

^eDepartment of Engineering, Lancaster University, Lancaster, LA1 4YW, UK

*Corresponding author: faridfcc2817@gmail.com

Abstract

The present study numerically investigates the optimization of thermal performance in a dimpled channel using a promising genre of nanofluid which is equipped with the inclusion of two-dimensional (2D) MXene (Ti_3C_2) nanoparticles to the Soybean Oil. The stream-wise and span-wise variation of the spherical dimples were kept 3.00 and 3.15 over the flow domain with an elongation of 2.5 mm. The detailed evaluation of both the local and global parameters are carried out for 0.025%, 0.075% and 0.125% weight concentrations of MXene. The Reynolds Number are varied from 1000 to 6000 to understand the effect of both the laminar and turbulent flow characteristics in predicting the thermal performance. The simulations are carried out using Finite Volume Method (FVM) under constant heat flux, assuming the mixture of nanoparticles as homogeneous mixture. The results show that with the increase in the weight concentration of nanoparticles, thermal performances of the nanofluid increases. However, it is also identified that with the increase in Reynolds Number, the thermal performance increases under turbulent flow regime. On the contrary, thermal performance was observed to be decreased with the increase in Reynolds Number under laminar flow regime. An astounding improvement of 88.9% thermal performance is found for 0.125% weight concentrations of Soybean based MXene nanofluid which exclusively indicates the credibility of MXene nanofluid as a next generation potential candidate for heat exchanger industries.

Keywords: MXene/Soybean oil nanofluid, CFD, Dimple Channel, Thermal Performance

1. Introduction

Improvement of thermal performance is one of the major technical challenges in many industries. For ensuring reliable thermal performance, effective cooling is highly desirable, which boosts the requirement of developing energy efficient methods to enhance adequate heat transfer, maintaining the lower cost of installations as well as maintenance. Among different techniques to enhance the heat transfer rate, active and passive methods are two mostly applied methods intrigued the industries. Active methods mostly deal with pulsation or pulsation of coolant, application of electrostatic fields etc. However, active methods require more power supply which might be unfavorable with industries. On the contrary, due to having lower requirement of cost as well as maintenance, passive methods are gradually becoming popular now a days. Passive methods mostly deal with the surface modification in order to increase the surface area for better heat transfer and intensifying the turbulence of the working fluid[1][2]. Insertion of twisted tapes, helically coiled wire, etc. towards the flow direction of working fluid, or increasing the surface roughness through creating dimples, protrusions, ribs, fins, corrugations etc. are the most noteworthy geometric modifications to activate passive methods for better thermal performance [3].

In accordance with the view of fluid dynamics, due to surface modifications like implementations of dimples, protrusions etc., the secondary flow, vortex, or swirling flow is generated which interrupts the boundary layer growths. This phenomenon leads to intensifying the turbulence intensity, which ultimately results in enhancement of heat transfer. Along with the increase of effective surface area, the repetitive circulation attachment and recirculation attachment of flow fields to the wall intrigues the augmentation of thermal performance [4][5].

Perwez et al. [6] investigated the effect of tear-drop and spherical dimpled surfaces in a rectangular channel varying the value of Reynolds Number from 14×10^3 to 65×10^3 following both numerical and experimental approach. The geometrical demonstration of such dimpled channel could be observed in **Figure 5**. The study revealed that rectangular channel with teardrop dimpled surface could increase the heat transfer up to 17% compared to spherical dimples. However, it was reported from the study that the friction factor also increased up to 16.14% due to the application of teardrop dimples compared to spherical one. Hence, a thorough study of thermal performance evaluation was required to provide a conclusion to claim the acceptability of teardrop dimples which was missing in the study. Chen et al. [7] performed an experimental investigation to evaluate thermo hydraulic characteristics of dimpled

surface in an annular channel using water as coolant under forced turbulent flow. An augmentation of heat transfer from 25% to 137% was observed from their study due to implementation of dimpled roughness compared to plain tube. In addition, Wang et al. [8] examined the effect of elliptical dimpled surface using water as working fluid and showed that with a cost of around 75% pressure drop, about 175% remarkable heat transfer enhancement was observed for dimpled tube compared smooth tube. García et al. [9] studied the effect of a wide range of artificial roughness which includes dimpled surface, corrugated surfaces, and helical wired coils under both laminar and turbulent flow conditions. The results concluded that the dimpled surfaces performed most considering the thermal performance compared to other investigated roughness when the value of Reynolds Number is above 2000. Li et al. [10] explored experimentally the thermo-hydraulic behavior of dimpled tube using water/glycol as coolant assuming single phase, varying Reynolds Number from 150 to 2000. The study concluded that formation of secondary flow, and interruption of boundary layers are the cause of increasing turbulence intensity, which resulted in the augmentation of heat transfer.

Traditional working fluid like water, oil, ethylene glycol etc. possesses lower heat transfer capacity which consequently prevent the improvement of thermal efficiency. Hence, another notable passive method to improve the thermal conductivity of working fluid was required to heat exchanger industries. Nanofluid comes up with a solution to the improvement of thermal efficiency. Inclusion of solid nanoparticles having mean diameter of 1-100 nm to the base fluid such as oil, water is called nanofluid which increases the thermal conductivity of the working fluid significantly.

Wen and Ding [11] investigated the performance of Al_2O_3 /water nanofluid under constant heat flux and concluded that with the increase in volume concentration of nanofluid and Reynolds Number, heat transfer rate enhances noticeably. They claimed that the reduction in the thermal boundary layer thickness and the random transportation of nanoparticles are the probable reason behind the enhancement. However, the evaluation of thermal performance and effectiveness of coolant were missing in the study. A developed correlation was provided by Li and Xuan [12] through experimental investigation for TiO_2 /water and Al_2O_3 /water under turbulent and laminar flow together. The study showed that considerable augmentation in heat transfer is possible with the implementation of nanofluid though the study did not concentrate on the effectiveness of the nanofluid. Maiga et al. [13] evaluated both the thermal and hydrodynamic behavior of Al_2O_3 /water and Al_2O_3 /EG nanofluid using numerical approach for a uniformly heated tube. The study showed that with the increase in volume fraction, the heat transfer rate increases. Additionally, the study also claimed that nanofluids affects the wall shear

stress unfavorably. However, the study did not evaluate the effectiveness of the nanofluid considering both heat transfer and pressure drop. Moreover, the study neglected the effect of variation of thermophysical properties due to change in temperature while investigating and assumed constant properties.

Considering the efficiency of the passive methods to upsurge the thermal performance, recent studies are biased to implement compound techniques for heat transfer enhancement which associates multiple passive methods or active and passive methods combined together [14]. Such compound techniques involve mostly modification of geometry as well as improvement in coolant. Li et al. [15] implemented dimpled and protrusion roughness over microchannel and Al_2O_3 -water as working fluid to evaluate the efficiency. The study showed that the thermal performance of the microchannel heat sinks improves considerably due to implementation of compound techniques. Moreover, the study assumed constant physical properties for thermofluid. Singh and Srivastava [16] experimentally evaluated the effect of Al_2O_3 -water nanofluid in dimpled channel and claimed that thermal boundary layers got flattened and the thickness of the boundary layer got reduced due to implementation of both the dimpled surface and alumina nanoparticles. Suresh et al. [17][18] investigated the heat transfer characteristics of spherical dimples with helical arrangement implementing CuO-water nanofluid as coolant under both the laminar and turbulent flow conditions. The conclusion claimed that both the implementation of nanofluid and dimpled surface plays a significant role in the augmentation of heat transfer and about 30% increase in thermal performance was recognized with the combination of both passive methods. However, the study did not focus upon the critical assessment of local parameters in heat transfer and pressure drop. Firoozi et al. [19] investigated the effect of different configured dimpled roughness in a circular channel using Al_2O_3 -water nanofluid as coolant varying Reynolds Number from 500 to 4000. The results concluded that with the increase in dimple height and decrease in the dimple pitch, the overall thermal performance got increased. Moreover, the maximum value of thermal performance was observed at higher volume fraction of Al_2O_3 -water nanofluid according to the study. Zheng et al. [20] experimentally investigated the heat transfer behavior and entropy generation of Al_2O_3 -water in a tube fitted with twisted tape adopted with dimpled surfaces. The results claimed that implementation of nanofluid along with enhanced effect of dimpled twisted tape drastically improves the heat transfer and decreases the entropy generation. The study implemented multiple passive methods which associate with twisted tape, dimple surface, and usage nanofluid and reached to an increase of 60% increase in thermal performance.

In the recent studies, MXene, a two-dimensional Nano-sheet material, is getting the attention due to having astounding thermo-physical properties. Because of having higher thermal conductivity and lower viscosity, MXene nanofluids found as better as coolants. Abdelrazik et al. [21] investigated the performance of water based MXene nanofluid in hybrid PV/T systems where the study concluded that MXene nanofluid with lower weight concentration provides better thermal performance in hybrid PV/T system. Bakthavatchalam et al. [22] investigated the thermal performance of MXene ionanofluids in hybrid PV/T solar systems, where the results showed a remarkable increase of 78.5% thermal efficiency due to implementation of MXene ionanofluids. Aslfattahi et al. [23] studied experimentally about the properties of Silicone oil based MXene nanofluid and implemented it as working fluid in photovoltaic solar thermal collector. The study claimed that due to application of MXene nanofluid, the electrical efficiency of the PV module is improved considerably because of better cooling.

Following the studies, it is pretty clear that MXene nanofluid based with both water and oils performed significantly better to improve both the thermal efficiency as well as electrical efficiency of hybrid PV/T solar systems. However, such a potential working fluid is not still implemented in the heat exchanger studies. Most of the compound techniques to enhance thermal performance are mostly associated with metallic nanofluids like Al_2O_3 -water, CuO-water etc. Moreover, though several works were carried out using Soybean oil as basefluid for different nanofluids in the field of thermal storage system and PV/T solar systems and reported better efficiency, the performance of such basefluid was not investigated at all till now in the field of heat exchanger industries [24][25]. The study achieved a remarkable improvement of about 89% thermal performance with the inclusion of tiny weight concentration of 0.125% MXene/Soybean nanofluid which is almost unlikely to be achieved by other traditional studies of nanofluid in heat exchanger studies upon the investigated cases. Upon investigating the literature study, it is pretty clear that application of multiple passive techniques including higher volume concentrations of metallic nanofluids could not reach such increase in the thermal performances of about 89%. Most of the metallic nanofluids which are common in heat exchanger studies were able to increase thermal performance below 50%. Moreover, the metallic nanofluids increase heat transfer coefficient with a loss of higher pressure drop. On the other hand, MXene/soybean nanofluid increased heat transfer of around 90.12% with the loss of 31.12% pressure drop. Such enhancement of heat transfer for the loss of only 31.12% pressure drop are unlikely for other nanofluids.

Most of the investigated studies uses constant properties of the coolant which might affect the conclusion of the study. Present study used temperature dependent thermophysical properties to claim trustworthy

conclusions. Moreover, those temperature dependent equations of thermophysical properties could be useful for other researchers to implement MXene/Soybean in the relevant studies.

It has to be noted that with the inclusion of only a tiny percentage of the MXene nanoparticles, such improvement in the thermophysical properties are unlikely in other nanofluids. Just with the inclusion of 0.125 wt% of MXene nanoparticles, about 23.34% improvement in thermophysical properties were achieved.

Hence, the objective of the present study is to associate compound techniques to improve thermal performance, where spherical dimpled channel with Soybean oil based MXene nanofluid would be investigated numerically implementing Finite Volume Method to solve the governing equations. Both application and evaluation of Soybean oil and MXene/Soybean oil would be carried out for the first time as a coolant in heat exchanger studies. The weight concentrations of MXene nanofluid would be varied from 0.025% to 0.125%. The thermophysical properties of Soybean oil and MXene/Soybean nanofluid are considered varying with the change of temperature to provide trustworthy conclusion on the application of such novel coolant. In order to understand the effect of flow behavior both the laminar and turbulent flow regime would be investigated. Moreover, heat transfer and pressure drop characteristics would be analyzed locally and globally to conclude the credibility of the MXene/Soybean oil nanofluid as a novel coolant in heat exchanger studies.

2. Thermo-physical Properties of MXene nanofluid

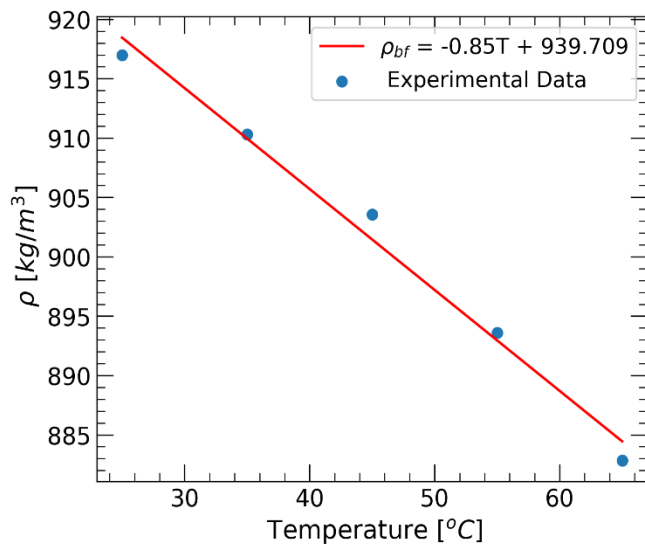
Though inclusion of solid particles in the base fluid makes the nanofluid a two-phase mixture, it might be doubtful whether the physics of traditional two phase flow could be implemented for nanofluid [26]. Nanofluids act like a fluid rather than to be a mixture due to inclusion of tiny sized particles [27][28]. A homogeneous model was proposed by Xuan and Roetzel [26] where the equations of convective transport theory for fluids are prolonged to nanofluids. Such phenomenon indicates that if the properties of pure fluids are exchanged with the properties of nanofluids, the conventional correlations of Nusselt Number could be used for nanofluids associated with weight concentration. However, several studies were continued predicting the mixture of nanoparticles as homogeneous mixture and assuming single-phase flow approach where the results align precisely with experimental investigations [29][30]. Moreover, Albojamal et al. [31] examined the performance of homogeneous single-phase approach, Discrete Phase Method (DPM), and Mixture Model in a circular channel using Al_2O_3 -water as working fluid. The study claimed that two-phase Mixture Model failed to predict the accurate thermo-hydraulic behavior of nanofluids. In addition, the study found a maximum discrepancy of 5.9% in between DPM approach and single-phase approach. Following the good agreement between the experimental results

and numerical predictions of several studies [32][33], the study suggested to implement single-phase approach while using temperature dependent thermophysical properties for the nanofluids while the volume fraction is less than 4% provided that the highest possible accuracy in thermo- physical properties is achieved for nanofluids.

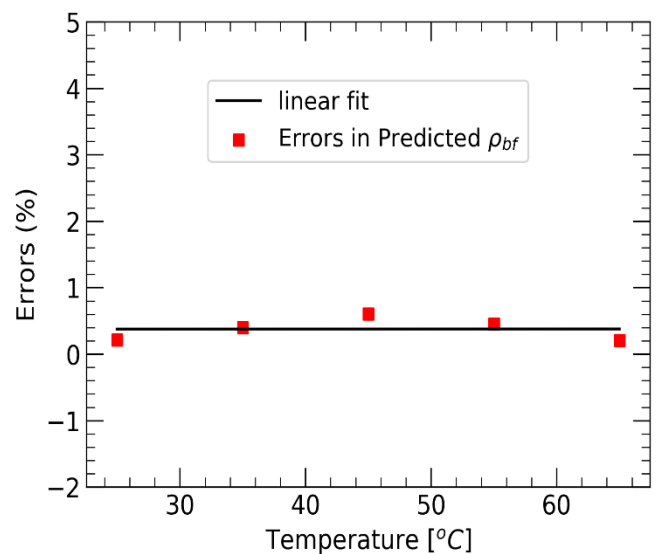
Hence, the present study assumed the mixture of MXene nanoparticles to the base fluid as homogeneous mixture and single-phase approach is taken into consideration. The thermo-physical properties of the MXene/Soybean (Ti₃C₂/SO) oil were taken from our previous the experimental study [34]. The data for thermal conductivity (k) and density (ρ) were taken and fitted into a linear curve approximation within the prescribed temperature limit of the study. The linear fitting approximation with the fitted equation were shown in **Figure 1 and Figure 2** for density and thermal conductivity respectively. **The linear equations for both thermal conductivity and viscosity, which are presented as a function of temperature in the figure, are used as User Defined Function (UDF) during numerical simulations. Moreover, the error analysis was also illustrated with the linear fit to understand the maximum and minimum deviations of the predicted thermal conductivity and density from the experimental study [34]. The errors were calculated following Equation 1. As identified from the Figure 1 and 2, the maximum deviations from the linear fitted equations are observed to be within 1% errors for density and within 2% errors for thermal conductivity respectively.**

$$Errors (\%) = \frac{P_{fitted} - P_{exp}}{P_{exp}} \times 100\% \dots\dots\dots (1)$$

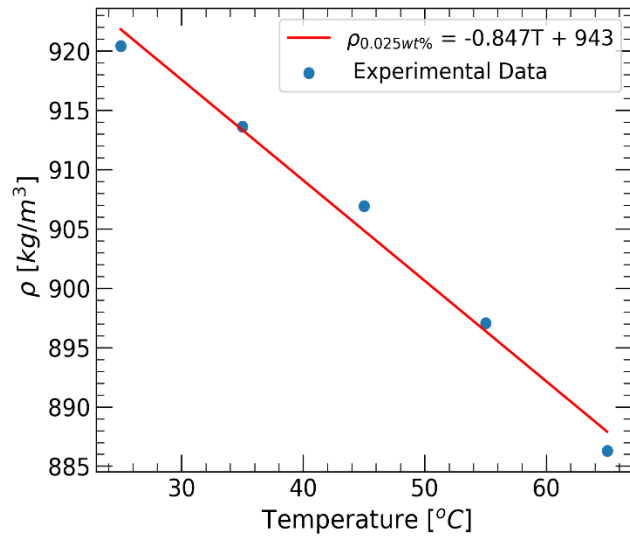
Where P_{fitted} represents the thermophysical properties predicted from fitted equations, P_{exp} represents the thermophysical properties from experimental study.



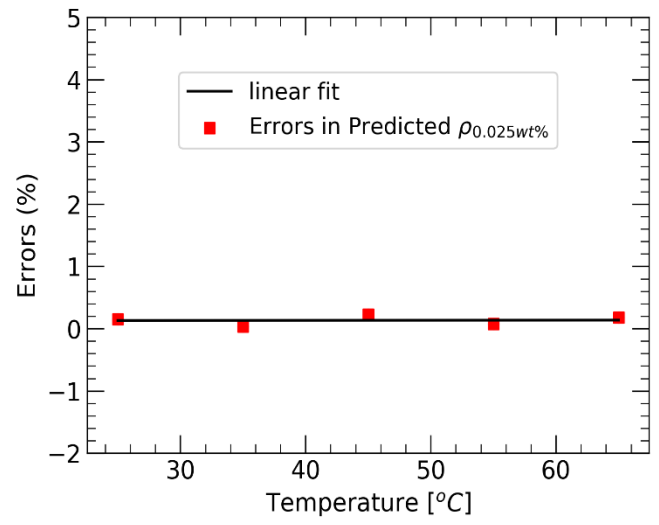
(a)



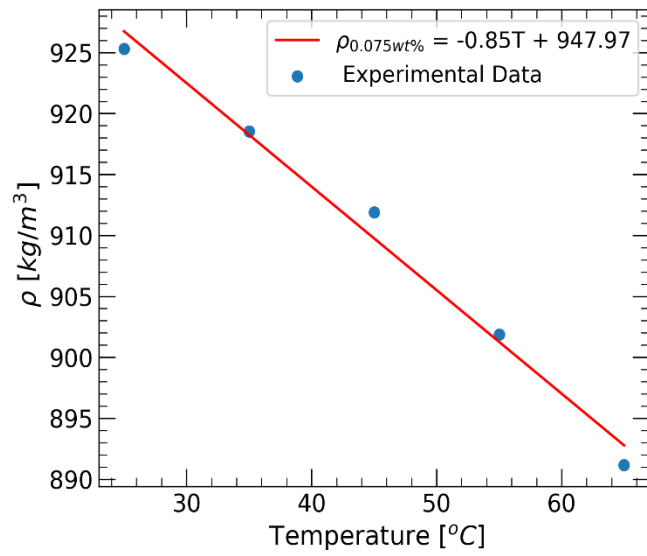
(b)



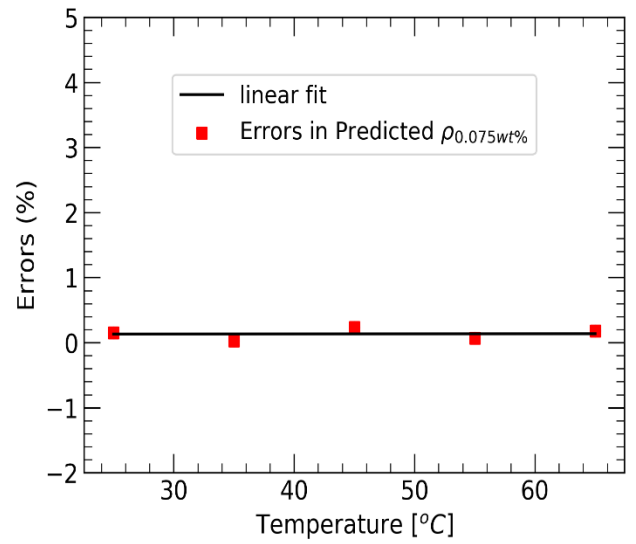
(c)



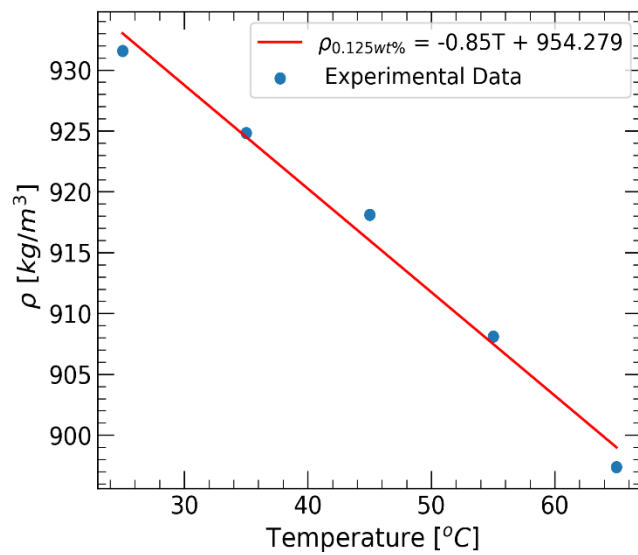
(d)



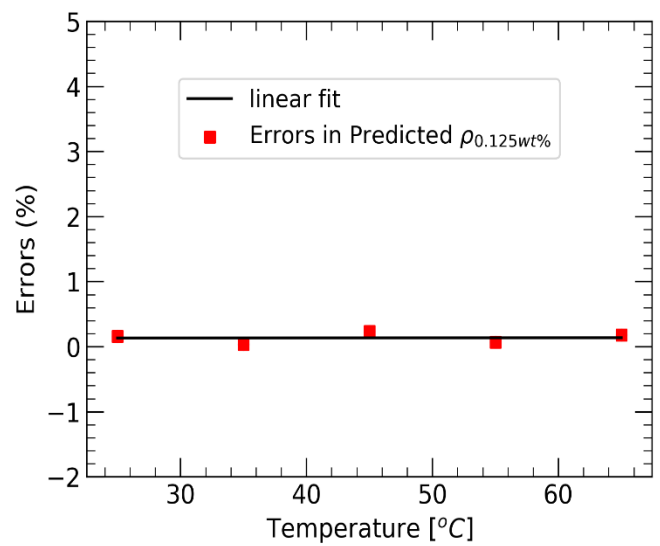
(e)



(f)

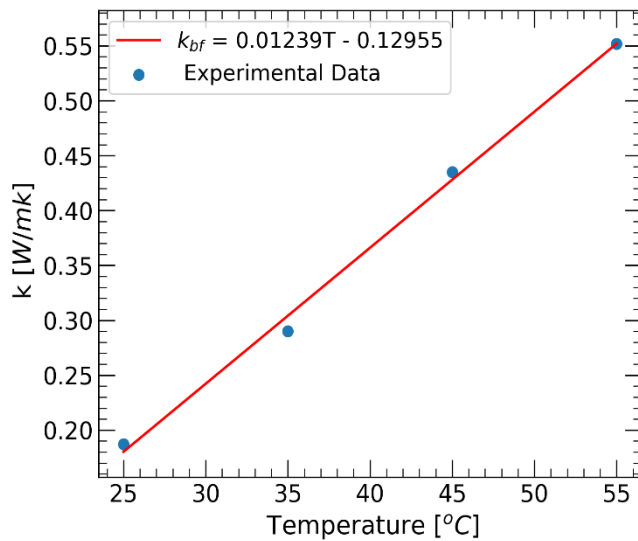


(g)

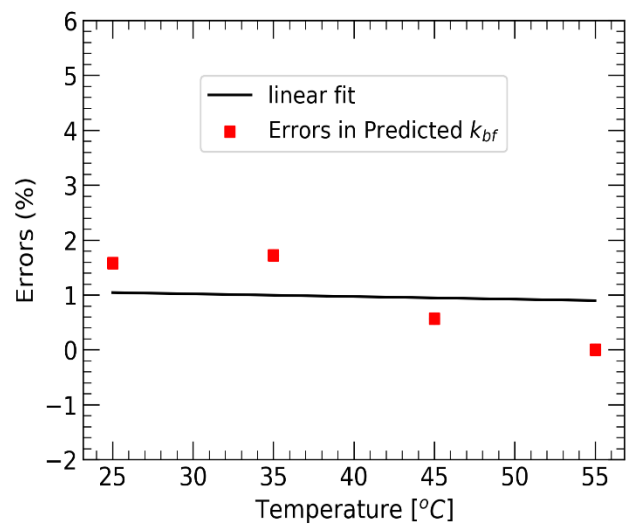


(h)

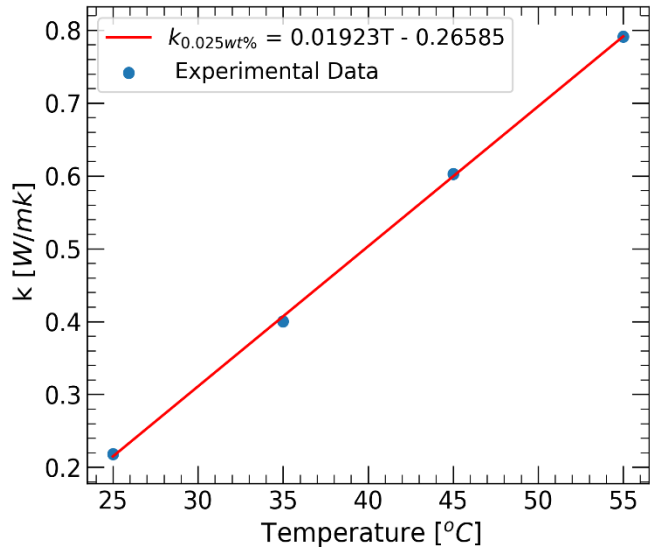
Figure 1: Linear curve fitting of density as a function of temperature and error analysis with linear fit from experimental study [34] for a) Soybean Oil b) 0.025 wt% c) 0.075 wt% d) 0.125 wt%



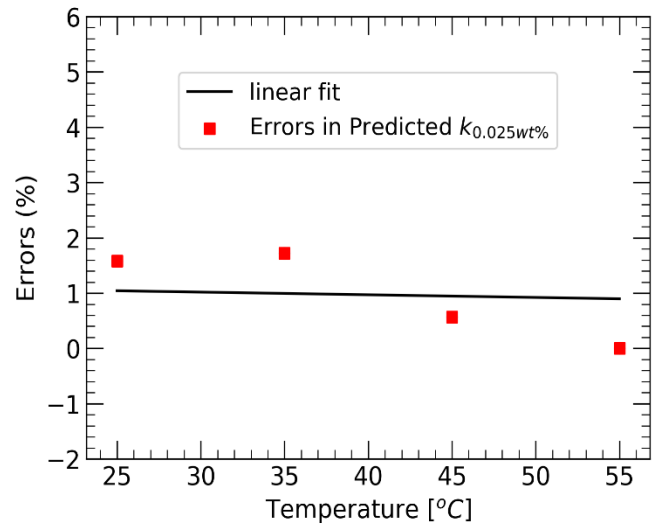
(a)



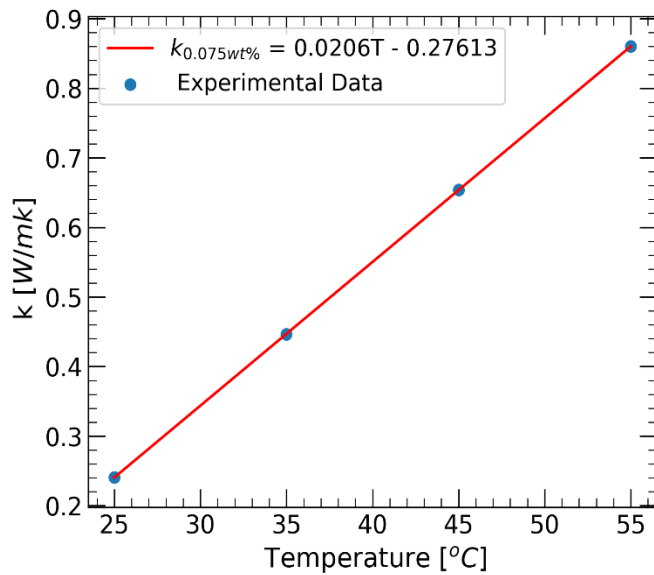
(b)



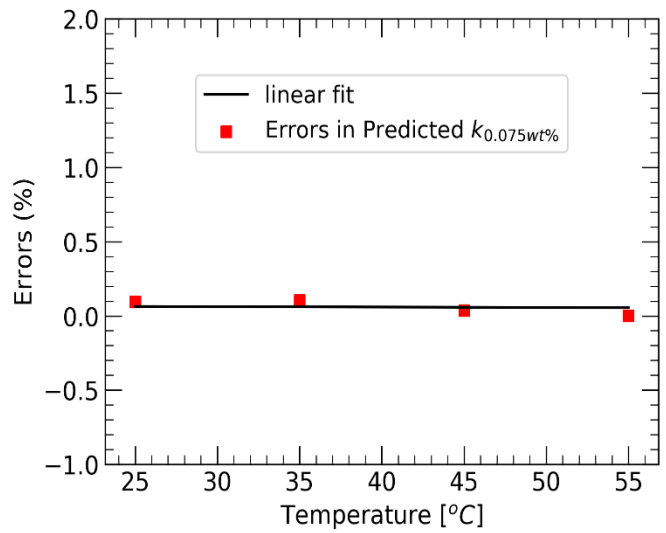
(c)



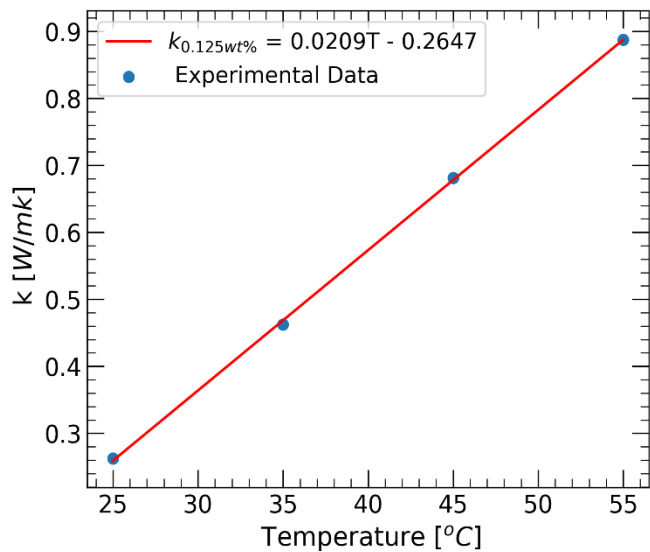
(d)



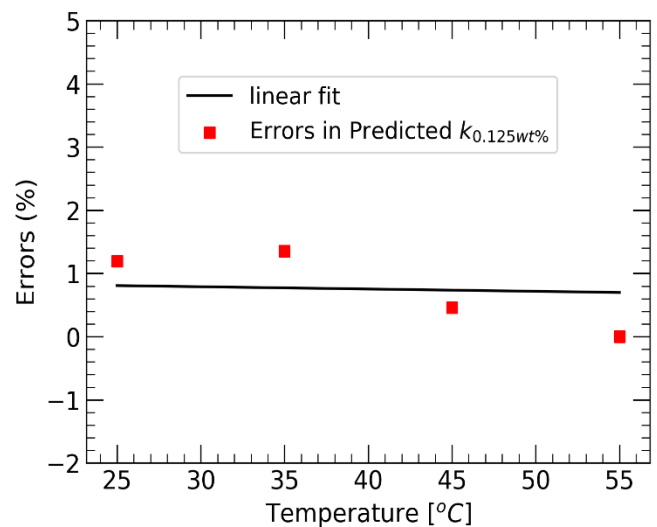
(e)



(f)



(g)



(h)

Figure 2: Linear curve fitting of thermal conductivity as a function of temperature and error analysis with linear fit from experimental study [34] for a) Soybean Oil b) 0.025 wt% c) 0.075 wt% d) 0.125 wt%

Since the experimental data of our study aligns precisely with the polynomial curve fitting, both the viscosity (μ) and specific heat (C_p) were assumed to be temperature dependent polynomial equation. The polynomial curve fitting of viscosity (μ) and specific heat (C_p) were represented in **Figure 3** and **Figure 4**. As evident from the figures, it is observed that the 4th order polynomial equations are capable of predicting the viscosity and specific heat with a good agreement. In addition, the errors encountered from the experimental data were evaluated in the Figure 3 and 4 with linear fit. It is identified from the figures that the maximum deviations encountered from the experimental study are about 1% for specific heat and 5.5% for viscosity consecutively.

Moreover, the temperature dependent polynomial fit are represented in Equations 2 and 3. Those polynomial equations are compiled during the numerical simulations through UDF (User Defined Function). In order to provide credible conclusions for MXene/SO nanofluid, the temperature dependent variant properties are adapted during the simulation and modelling.

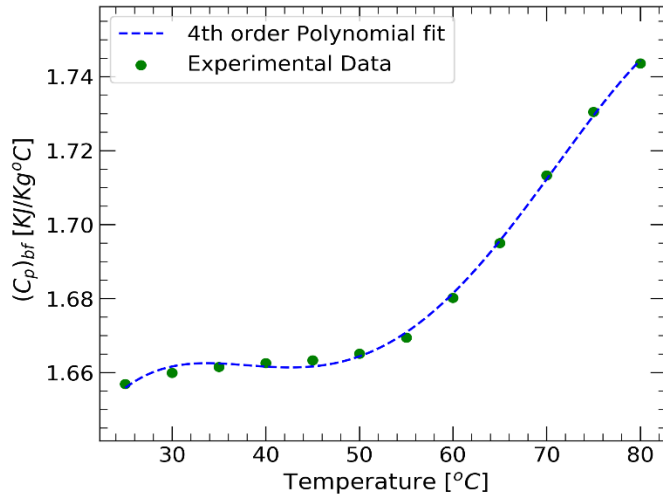
Specific heat (C_p) of thermofluids:

$$(C_p)_{bf} = -4.986 \times 10^{-8} T^4 + 1.09 \times 10^{-5} T^3 - 8.09 \times 10^{-4} T^2 + 2.51 \times 10^{-2} T + 1.385 \dots\dots\dots (2a)$$

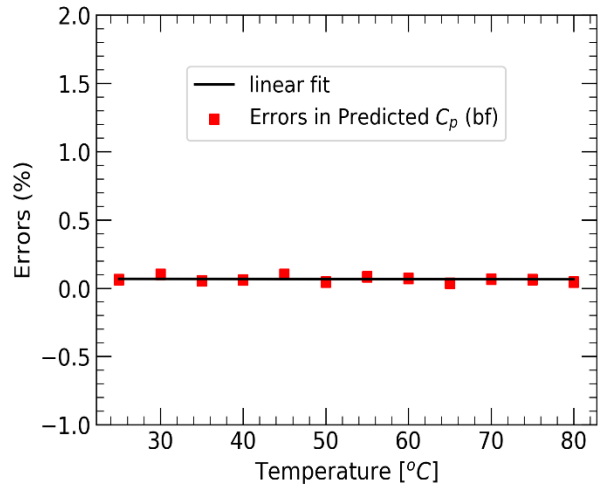
$$(C_p)_{0.025 \text{ wt}\%} = -3.27 \times 10^{-8} T^4 + 7.26 \times 10^{-6} T^3 - 5.12 \times 10^{-4} T^2 + 1.362 \times 10^{-2} T + 1.568 \dots\dots\dots (2b)$$

$$(C_p)_{0.075 \text{ wt}\%} = -1.78 \times 10^{-6} T^3 + 2.87 \times 10^{-4} T^2 - 1.04 \times 10^{-2} T + 1.93 \dots\dots\dots (2c)$$

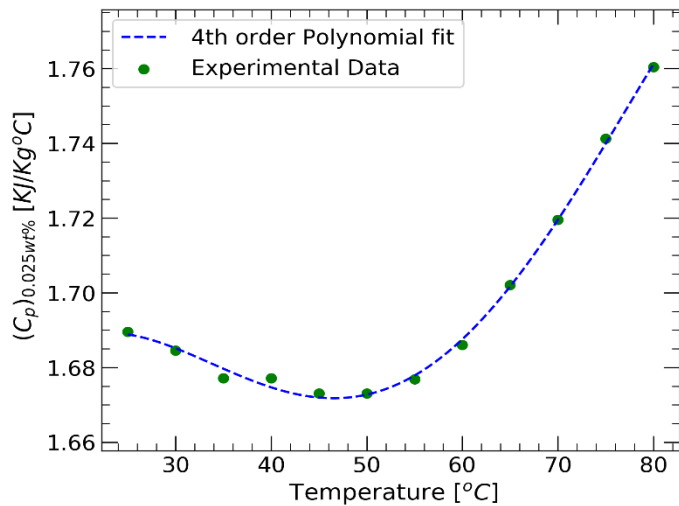
$$(C_p)_{0.125 \text{ wt}\%} = 2.13 \times 10^{-6} T^3 - 2.44 \times 10^{-4} T^2 + 7.286 \times 10^{-3} T + 2.00 \dots\dots\dots (2d)$$



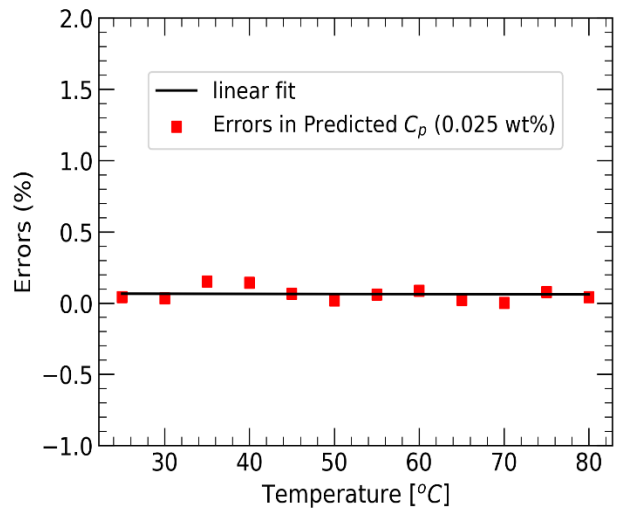
(a)



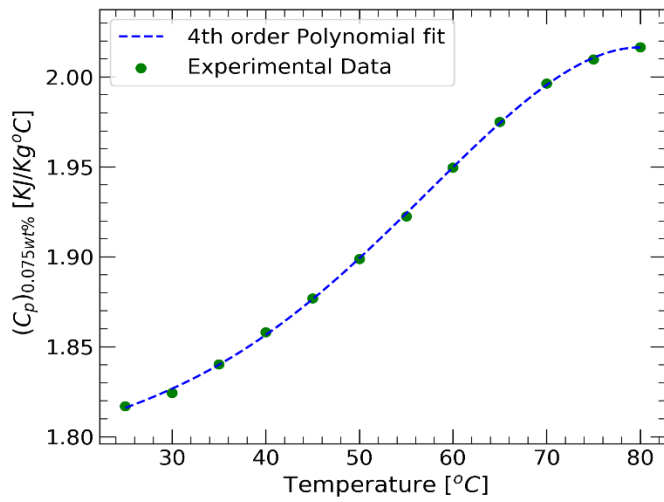
(b)



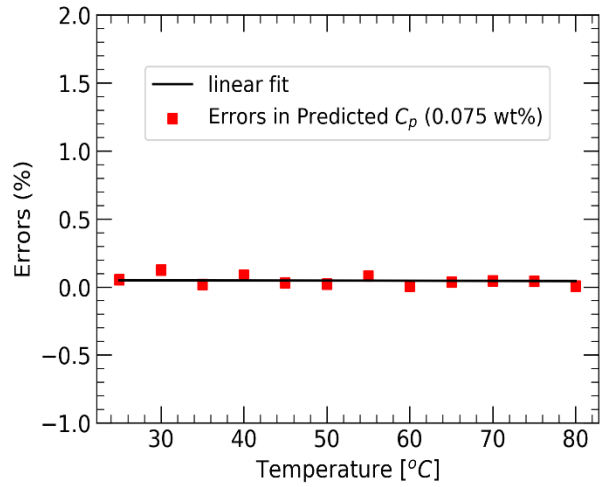
(c)



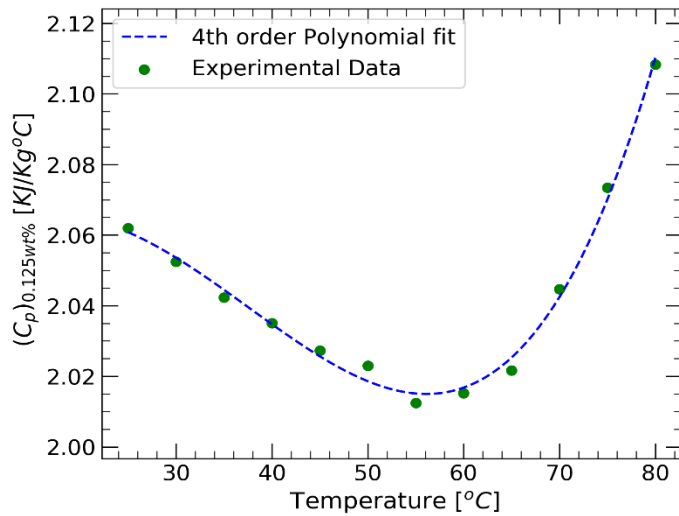
(d)



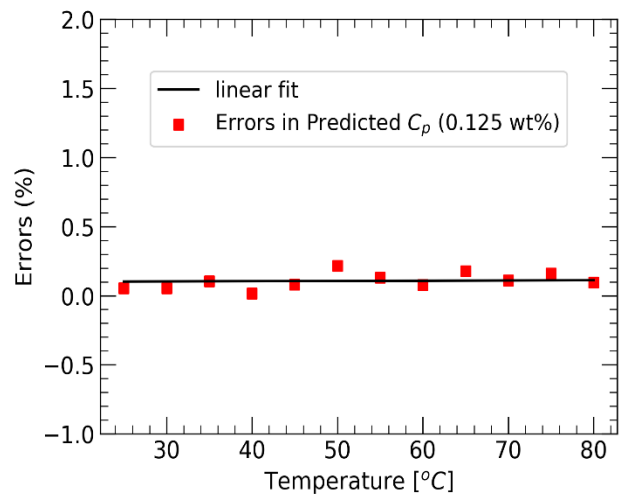
(e)



(f)



(g)



(h)

Figure 3: Polynomial curve fitting of specific heat as a function of temperature and error analysis with linear fit from experimental study [34] for a) Soybean Oil b) 0.025 wt% c) 0.075 wt% d) 0.125 wt%

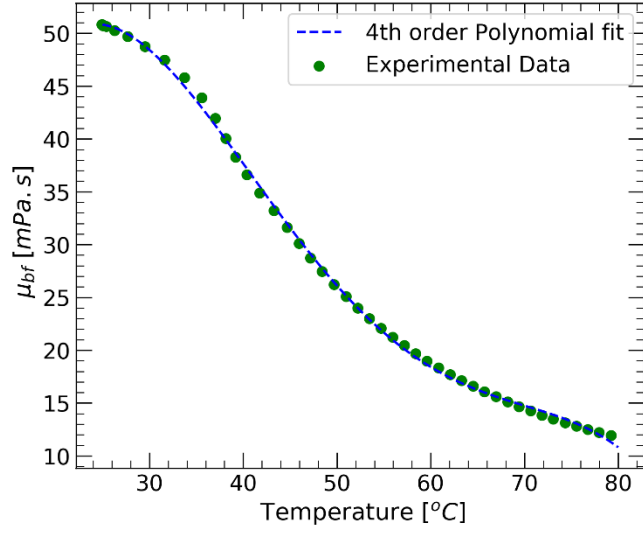
Viscosity of thermofluids:

$$\mu_{0.125 \text{ wt}\%} = -2.28 \times 10^{-5} T^4 + 5 \times 10^{-3} T^3 - 3.85 \times 10^{-1} T^2 + 1.13 \times 10^1 T - 5.23 \times 10^1 \dots \dots \dots (3a)$$

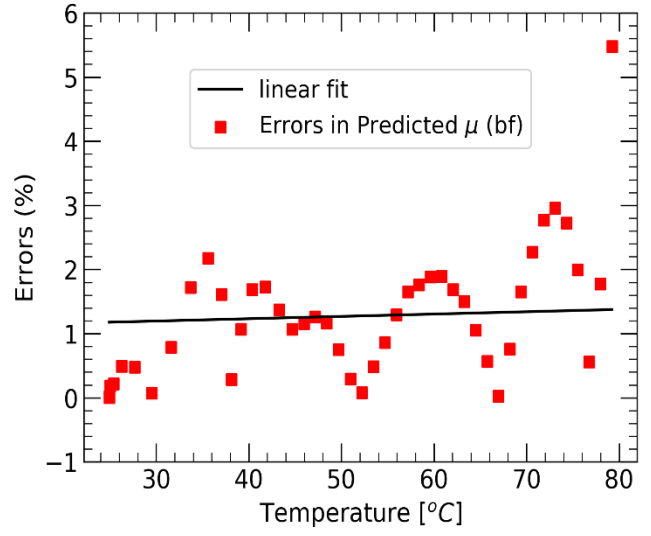
$$\mu_{0.075 \text{ wt}\%} = -2.2 \times 10^{-5} T^4 + 4.9 \times 10^{-3} T^3 - 3.80 \times 10^{-1} T^2 + 1.13 \times 10^1 T - 5.59 \times 10^1 \dots \dots \dots (3b)$$

$$\mu_{0.025 \text{ wt}\%} = -2.19 \times 10^{-5} T^4 + 4.88 \times 10^{-3} T^3 - 3.80 \times 10^{-1} T^2 + 1.13 \times 10^1 T - 5.67 \times 10^1 \dots \dots \dots (3c)$$

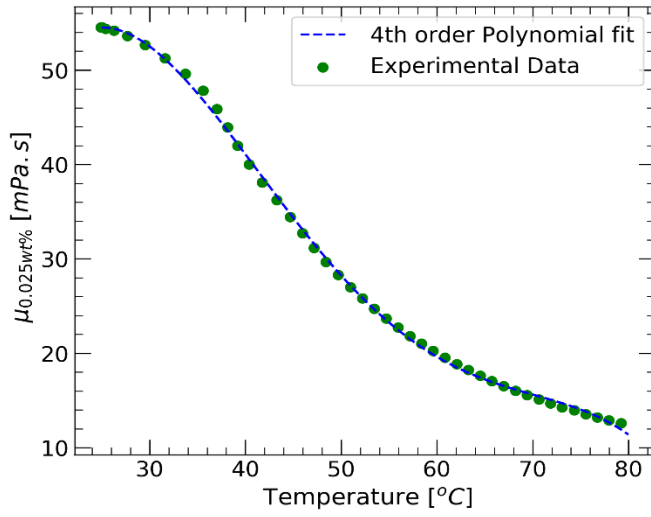
$$\mu_{bf} = -1.87 \times 10^{-5} T^4 + 4.14 \times 10^{-3} T^3 - 3.20 \times 10^{-1} T^2 + 9.25 T - 3.80 \times 10^1 \dots \dots \dots (3d)$$



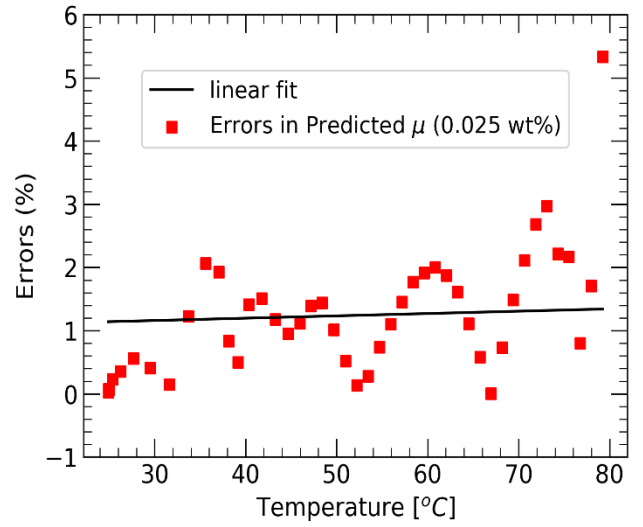
(a)



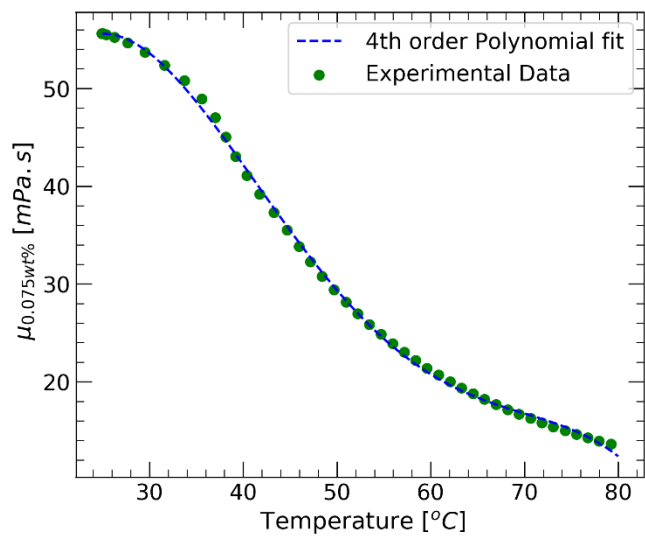
(b)



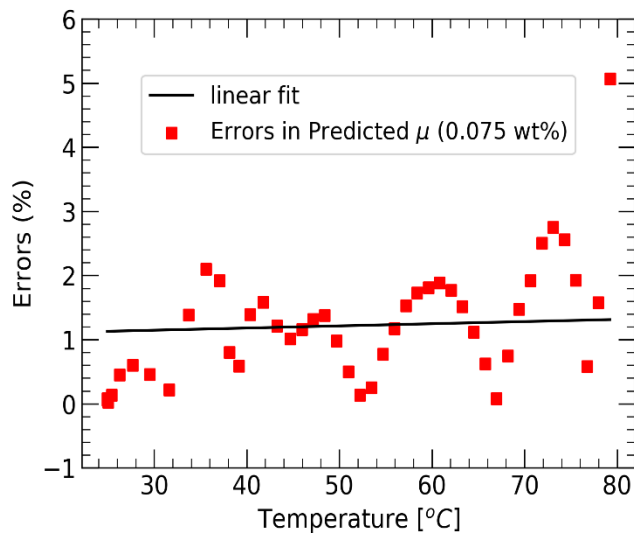
(c)



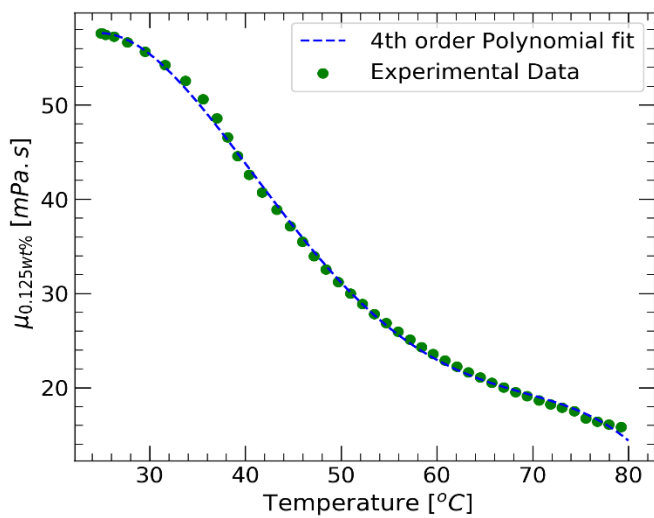
(d)



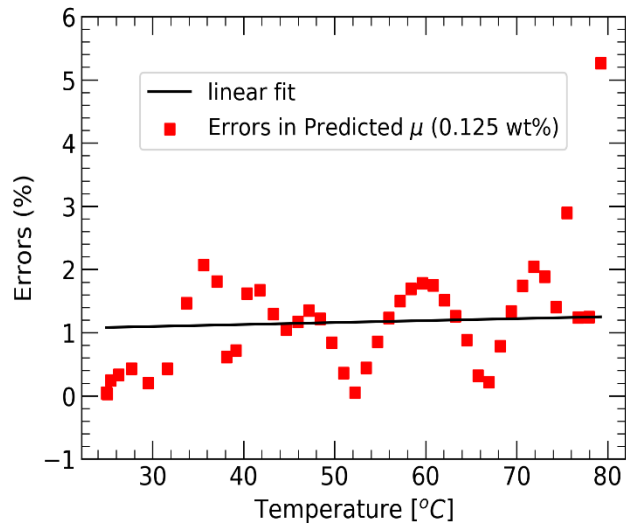
(e)



(f)



(g)



(h)

Figure 4: Polynomial curve fitting of viscosity as a function of temperature and error analysis with linear fit from experimental study [34] for a) Soybean Oil b) 0.025 wt% c) 0.075 wt% d) 0.125 wt%

3.1 Geometrical configuration

The length (L) of the flow channel is taken to be 1000 mm with hydraulic diameter (D) to be 45 mm. The depth of the spherical dimples over the smooth channel (e) was considered 2.5 mm. The diameter (d) of the spherical dimples were taken as 5 mm and the dimples were arranged parallel to each other. The Span wise distance (y/d) was considered as 3.15 whereas the Stream wise distance (x/d) was taken as 3.0 for the investigation of present study of dimpled channel. **Figure 5** and **Figure 6** display the geometrical configuration of the investigated study.

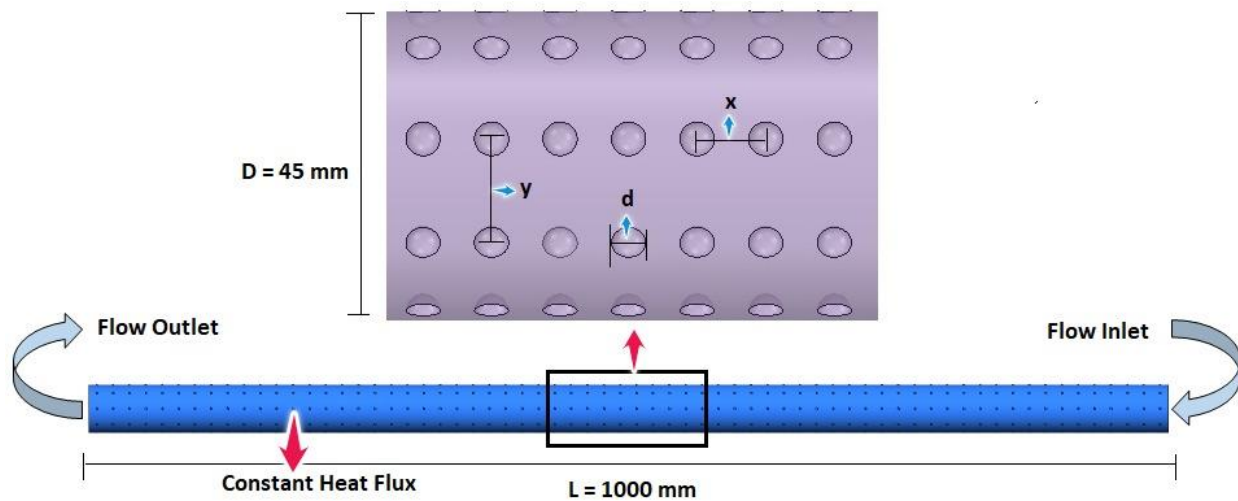


Figure 5: Demonstration of Computational Geometry

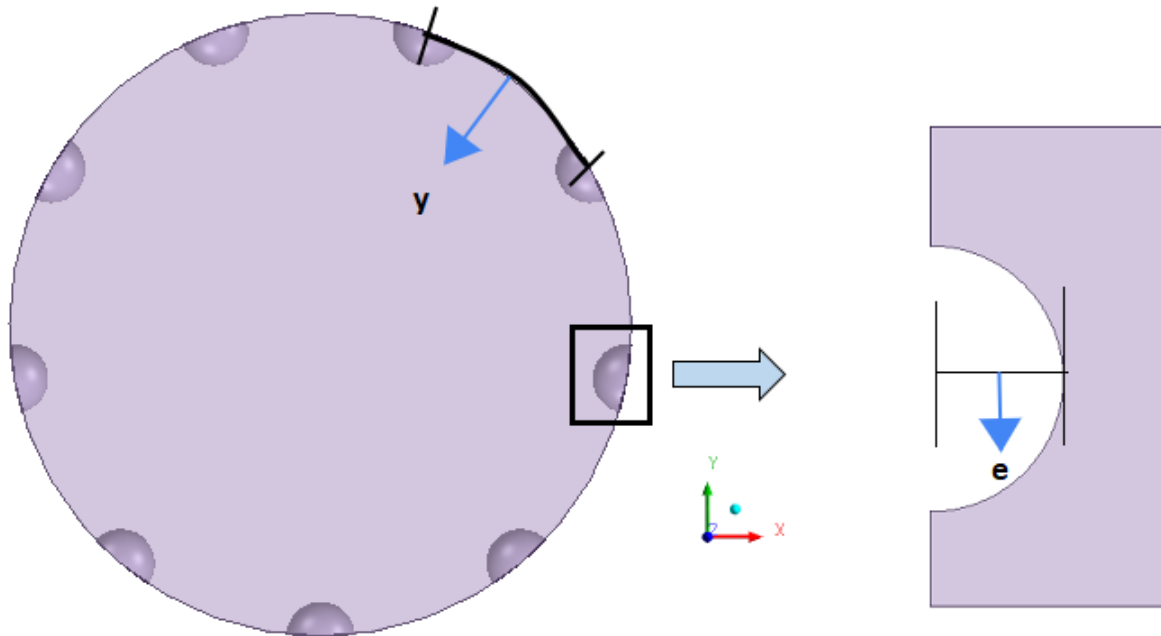


Figure 6: Radial View of Computational Geometry

3.2 Governing Equations

Assumptions during Numerical Investigations:

- 1) The coolant was assumed to be a Newtonian Fluid during numerical investigations. Since the thermofluid is considered as Newtonian fluid, the ratio of stress rate and strain rate is constant
- 2) Since the thermo-fluid is considered as Newtonian Fluid the viscosity is taken to be independent of shear rate [35].
- 3) The mixture of nanoparticles to the base fluid is considered to be homogeneous mixture with uniform dispersions of the particles [36][37]. Henceforth, the velocity of the solid nanoparticle was assumed equal to the velocity of the basefluid.
- 4) The numerical simulations were carried out under steady state condition.

The simulations are carried out under both forced laminar and turbulent conditions. Finite Volume Method (FVM) was implemented as solving procedure to solve 3D Navier-Stokes equation. The governing equations are showed below [38][39]:

Continuity Equation:

$$\frac{\partial \rho_{nf}}{\partial t} + \nabla \cdot (\rho_{nf} \vec{v}) = 0$$

..... (4)

Momentum Equation:

$$\frac{\partial (\rho_{nf} \vec{v})}{\partial t} + \nabla \cdot \rho_{nf} \vec{v} \vec{v} = -\nabla P + \nabla \cdot \vec{\tau} + \rho_{nf} \vec{g}$$

..... (5)

Energy Equation:

$$\frac{\partial (\rho H)}{\partial t} + \nabla \cdot (\rho H \vec{v}) = -\nabla \cdot \vec{q} + \dot{q}''' - P \nabla \cdot \vec{v}$$

..... (6)

Kumar et al. [40] investigated the performance of different turbulence model for spherical dimpled channel with similar geometrical configuration, compared the results and concluded that RNG k-ε model is mostly prominent to draw precise results. Besides, Ahmed et al. [37][41] also compared the performances of different turbulent model for internal flows in triangular array of rod bundles, and showed that RNG k-ε model is enough suitable to predict accurate results. Hence, in the present study, the evaluation of forced turbulent flows were carried out using RNG k-ε model. Equation (7) and Equation (8) represents the equations of RNG k-ε model.

$$\frac{\partial}{\partial t} (\rho k) + \frac{\partial y}{\partial z_i} (\rho \epsilon u_i) = \frac{\partial}{\partial z_j} \left(\alpha_k \mu_{eff} \frac{\partial k}{\partial z_j} \right) + G_k + G_b - \rho \epsilon - Y_M + S_k$$

..... (7)

$$\frac{\partial}{\partial t} (\rho \epsilon) + \frac{\partial y}{\partial x_i} (\rho \epsilon u_i) = \frac{\partial}{\partial z_j} \left(\alpha_k \mu_{eff} \frac{\partial k}{\partial z_j} \right) + C_{1\epsilon} \frac{\epsilon}{k} (G_k + C_{3k} G_b) - C_{2\epsilon} \rho \frac{\epsilon^2}{k} - R_\epsilon + S_\epsilon$$

..... (8)

The values of model constant, C_{1ε} and C_{2ε} are chosen to be 1.42 and 1.68 according to the following ANSYS Theory Guide [37][40][42].

3.3 Generation of Mesh and Sensitivity Analysis

Generation of grids over the geometry plays an important role in Finite Volume Method for the convergence of the solution. Hexahedral meshes were generated over smooth channel with enhanced wall treatment. Inflation layers were generated near the wall to capture the flow separations and thermal gradient precisely. The skewness factor and the orthogonal quality was kept 0.11 and 0.92 respectively. However, in order to justify the performance of hexahedral mesh over tetrahedral and polyhedral mesh, a comparison study was provided among the grids in **Figure 7**. The magnitude of element size was varied from 0.005 m to 0.001 m. As observed from the figure, higher the magnitude of the element size greater the discrepancy from the Dittus-Boelter study presented in **Equation 14** for all cells. When the element size is large, the performance of hexahedral cell is lower compared to polyhedral and tetrahedral cells. However, with the decrease of element size such discrepancies are diminished and at 0.001m element size each type of cells approached to the accuracy, showing a good agreement with Dittus-Boelter study. Considering the computational efforts, hexahedral mesh were chosen for the smooth channel. **Figure 8** shows the grid generation over the smooth channel.

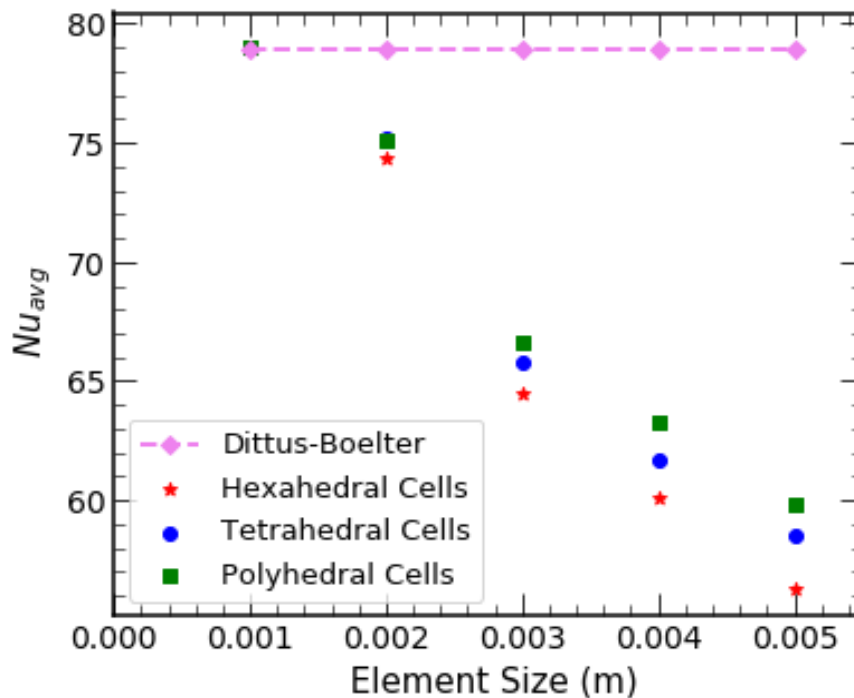
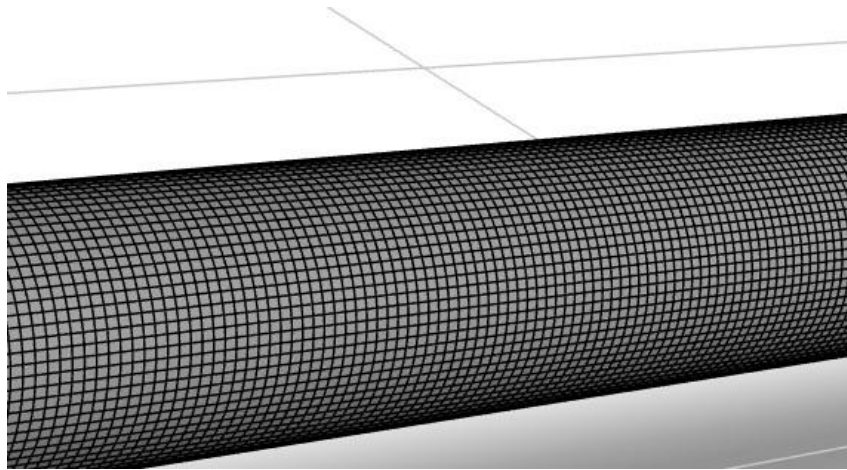
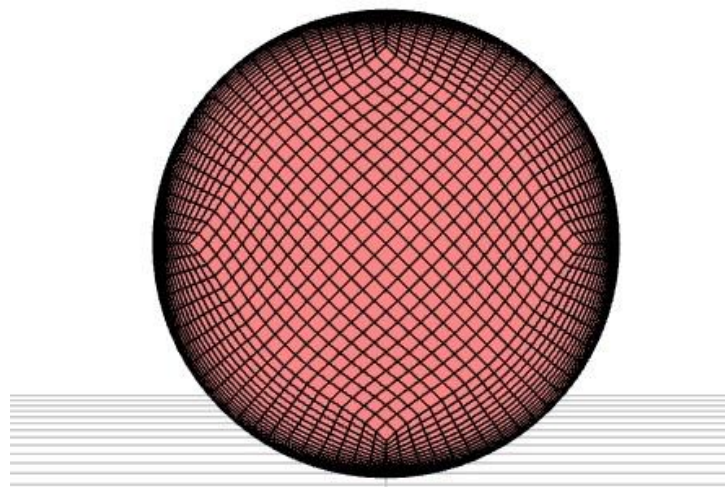


Figure 7: Evaluation of different types of grid on smooth channel



(a)



(b)

Figure 8: Illustration of Grid Generation for smooth channel (a) Over wall (b) Along Radial Plane

Considering the accuracy of the solution, polyhedral meshes were generated over the dimpled channel with enhanced wall treatment. The skewness factor of the geometry was kept 0.15 where as the orthogonal quality was maintained to be 0.88. In order to ensure high wall treatment, the value of Y^+ was maintained as +1, which provided the assurance to capture the viscous sub-layer of Turbulence Model. During the generation of inflation layers, the value of first node of boundary layers were chosen in such a way that

it ensures the value of Y^+ to be +1. RNG k- ϵ model was implemented during calculation with enhanced wall function to capture the velocity gradient and thermal boundary layer precisely.

In addition, similar to previous approach, a comparison among different types of grids were studied varying element size from 0.005 m to 0.001 m for the dimpled channel. As shown in **Figure 9**, the accuracy of the computational domain increases as the magnitude of element size decreases. Moreover, it is identified that polyhedral mesh performs best and aligned with the results of Maithani & Kumar[44] precisely for the dimpled channel. Hence, polyhedral grids were selected for the dimpled channel. Moreover, the element size and the node numbers play a significant role to predict the numerical results. In addition, implementation of polyhedral meshes also demand for higher computational efforts. Hence the evaluation of optimized mesh is necessary with the help of mesh independence test. Varying the number of nodes according to refinement of the meshes, the variation of Nu was observed. **Figure 10** represents the grid convergence index and mesh sensitivity of the dimpled channel. It is observed from the figure that variation of Nu gradually diminishes with the increase in node numbers and tends to flatten at 2.3 million. Since the value of Nu does not change with the increase in node numbers beyond 2.4 million, the mesh over the computational domain with 2.4 million node number was chosen to be optimized mesh for the present study. **Figure 11** shows the polyhedral grid generations over the dimpled channel and **Figure 12** shows the illustration of Y^+ value for the dimpled channel.

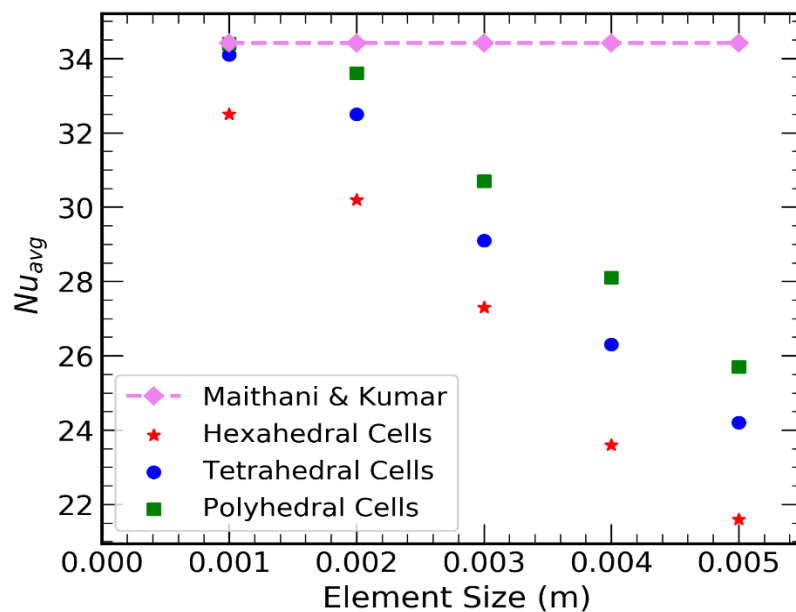


Figure 9: Evaluation of different types of grid on dimpled channel

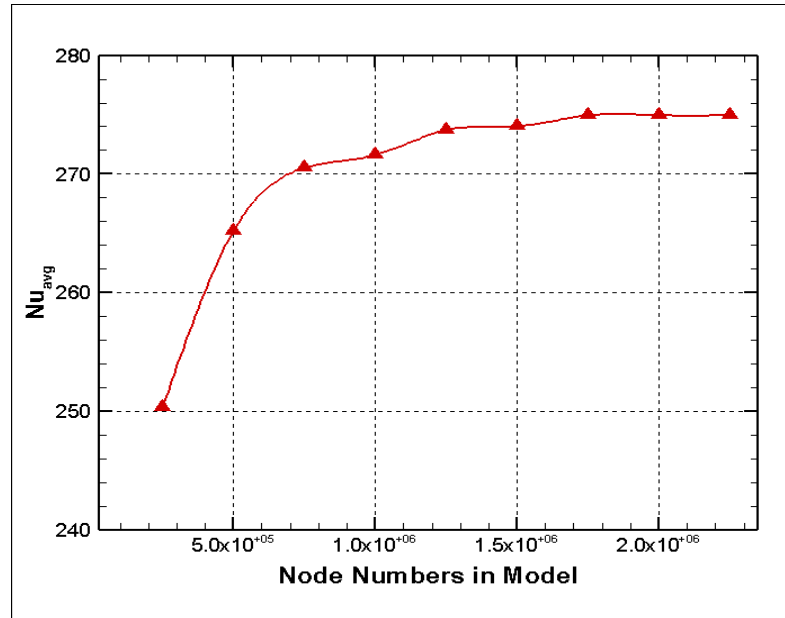
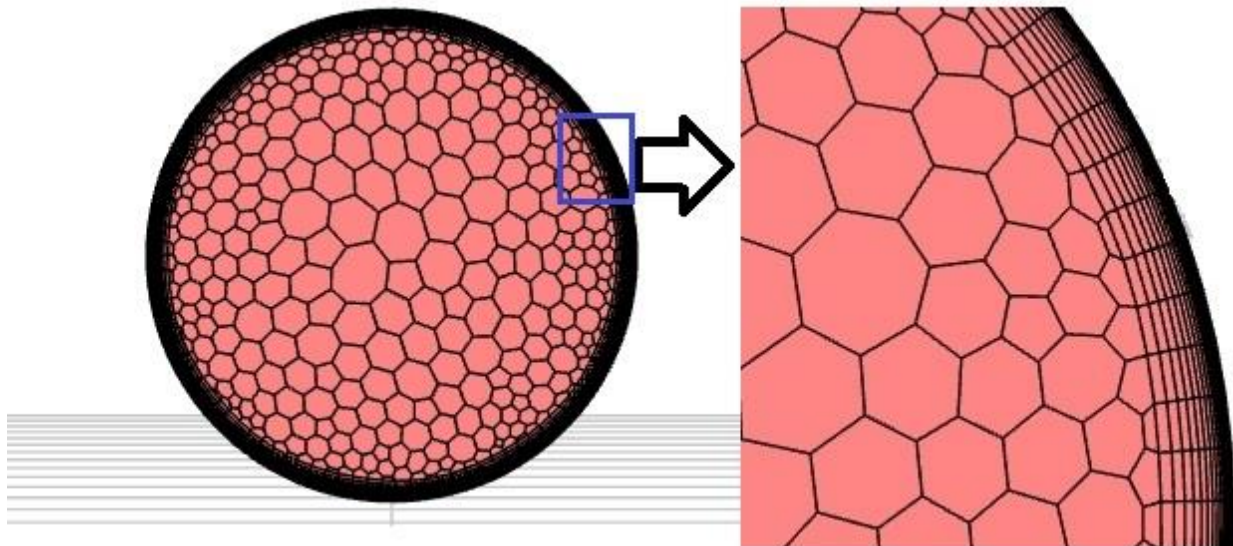
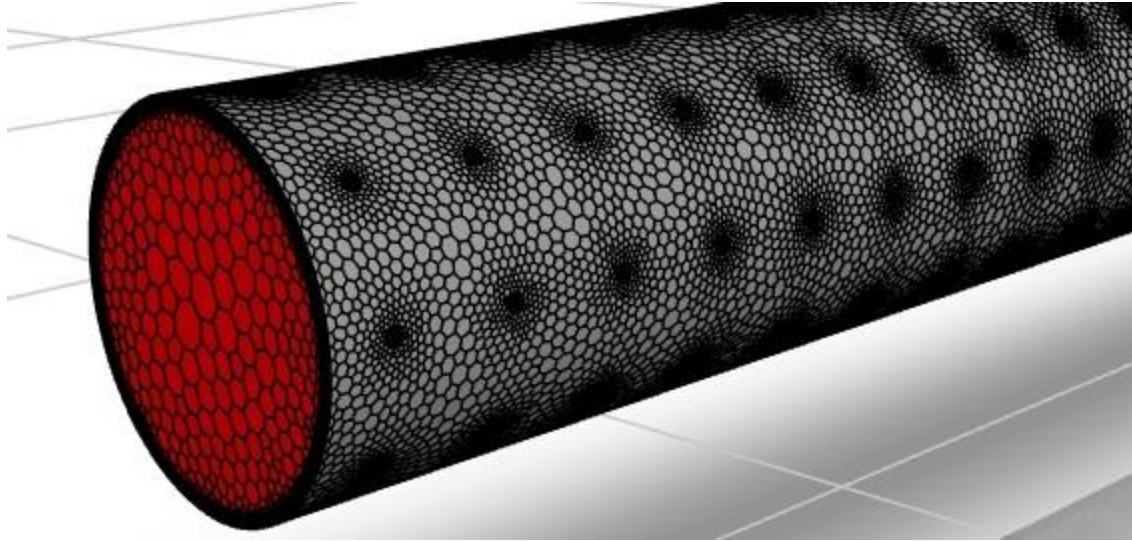


Figure 10: Analysis of Mesh Sensitivity and Grid Independence in Dimpled Flow Regime



(a)



(b)

Figure 11: Generation of grid over the dimpled channel (a) Over Radial Plane (b) Over the wall

Wall Yplus

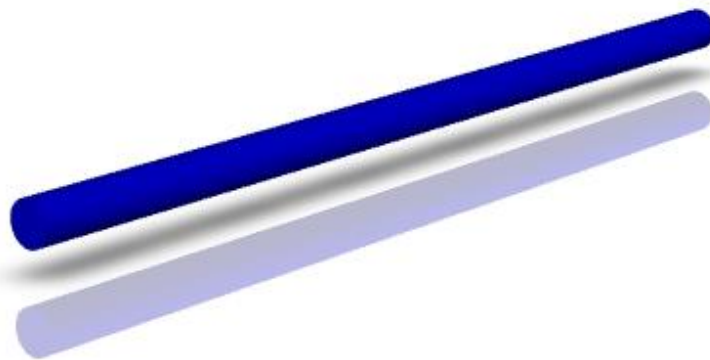
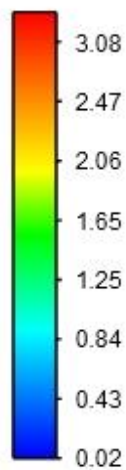


Figure 12: Evaluation of the value of Y+ over the dimpled channel

3.4 Boundary Conditions and Solving Procedure

A constant and uniform heat flux of 50kW/m^2 was applied to the wall of the investigated geometries. The inlet temperature of the geometry was chosen as 298K whereas at outlet gauge pressure was considered as zero. For evaluating the impact of both laminar and turbulent flow over the investigated geometries, the value of Re was varied from 1000 to 6000.

The mathematical representation of the boundary conditions for the computational domain are presented as below:

At the inlet (Z=0):

$$T = T_{\text{inlet}} (298\text{K}); V_{\text{radial}} = V_{\text{tangential}} = 0; V_{\text{axial}} = V_{\text{in}} \text{ (According to Re);}$$

At the outlet (Z=L)

$$\frac{\delta V_{\text{radial}}}{\delta z} = \frac{\delta V_{\text{tangential}}}{\delta z} = \frac{\delta V_{\text{axial}}}{\delta z} = 0; \frac{\delta T}{\delta z} = 0$$

At the wall (r=r_{outer wall})

$$V_{\text{radial}} = V_{\text{tangential}} = V_{\text{axial}} = 0; q'' = 50\text{kW/m}^2 \text{ (Constant)}$$

At the solid-fluid interface (Dimple wall to coolant interface)

$$V_{\text{radial}} = V_{\text{tangential}} = V_{\text{axial}} = 0; -k \frac{\delta T}{\delta r} = q'' = 0$$

Implicit Solver was implemented to solve governing equations. For obtaining pressure field, SIMPLEC algorithm was selected for pressure velocity coupling. Second order upwind discretization was implemented for mass conservation, continuity, momentum and energy equations whereas first order upwind discretization was selected for both turbulence kinetic energy and turbulence dissipation rate. The convergence criteria were set through residual monitoring. The scaled residual values for the continuity, momentum and x, y, z velocity were kept e⁻⁶ and for the energy the scaled residual values were kept e⁻⁸. The numerical investigations were carried out commercial computational fluid dynamics software ANSYS Fluent.

4. Data Reduction

$$\text{Re} = \frac{\rho v D_h}{\mu} \dots\dots\dots (9)$$

Where ρ represents the density of the coolant, v represents the velocity of the coolant, μ represents viscosity of the coolant and D_h represents the hydraulic diameter of the channel.

$$h(z) = \frac{q''}{T_{z(w)} - T_{z(b)}} \dots\dots\dots (10)$$

Where q'' illustrates the constant heat flux, T_{z(w)} and T_{z(b)} shows the wall temperature and bulk temperature of the fluid along the direction of flow.

$$\bar{h} = \frac{1}{L} \int_0^L h(z) dz \dots\dots\dots (11)$$

Where \bar{h} (h_{avg}) is the average heat transfer coefficient of the fluid, L is the flow length of the channel

$$\overline{Nu} = \frac{\bar{h} \times D_h}{k_o} \dots\dots\dots (12)$$

Where \overline{Nu} (Nu_{avg}) is the averaged nusselt number and k_o is the thermal conductivity of the fluid at inlet temperature.

$$f = \frac{2 \times \Delta P_{avg} \times D_h}{4 \times \rho \times L \times v^2} \dots\dots\dots (13)$$

Where, f represents the friction coefficient, ΔP_{avg} represents the averaged pressure drop of coolant, and v represents the coolant velocity.

5. Validation of the Model

In order to validate the smooth channel, Dittus-Boelter [43] correlations for Nu and Blasius correlation for friction coefficient were used to compare the numerical results investigated in the present study. Following exactly same boundary conditions, water as a coolant was investigated in the smooth channel to justify the numerical predictions achieved by smooth domain. Equation 14 and Equation 15 show the Dittus-Boelter and Blasius correlation with the applicable ranges and conditions. **Figure 13** shows the comparison of the present study with the correlations. It is evident from the figure that, the numerical results of the present study aligns precisely with a good agreement to both the correlations provided by Dittus – Boelter and Blasius. The maximum error of 3.8% was identified for Nu_{avg} from Dittus-Boelter correlation at Re 3000 whereas the maximum discrepancy of 2.83% was identified for f_{avg} from Blasius equations at Re 6000.

$$Nu = 0.024 Re^{0.8} Pr^{0.4} \dots\dots\dots (14)$$

$0.5 < Pr < 120, 6.0 \times 10^3 < Re < 1.0 \times 10^7$

$$f = \frac{0.3164}{Re^{0.25}} \dots\dots\dots (15)$$

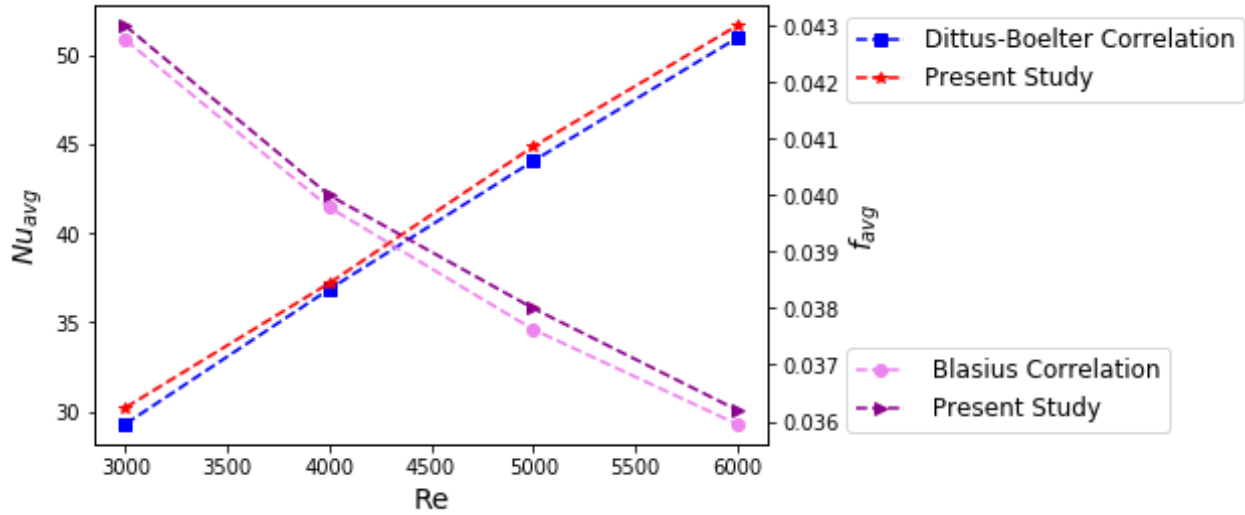


Figure 13: Comparison of Nu_{avg} and f_{avg} for Smooth Channel with traditional correlations

The credibility of dimpled flow regime was carried out following the experimental correlations developed for both Nu_{avg} and f_{avg} by Maithani & Kumar [44] as they developed the correlations for similar geometrical configurations. Equation 16 and Equation 17 show the correlations for Nusselt number and friction coefficient respectively. Noted that, following the same boundary conditions, air as a coolant was implemented during validation study since the correlations developed by Maithani & Kumar are valid only for air. It is identified from the **Figure 14** that the present study aligns precisely with the experimental studies of Maithani and Kumar. The maximum discrepancy of 1.20% was found for Nusselt number whereas maximum error of 4.80% was observed for friction coefficient from the experimental study of Maithani & Kumar.

$$Nu = 2.98 \times 10^{-3} Re^{0.9899} \left(\frac{y}{d}\right)^{1.3085} \exp(-2.48 \ln(\frac{y}{d}))^2 \left(\frac{x}{d}\right)^{-0.1754} \exp(-0.004 \ln(\frac{x}{d}))^2 \left(\frac{e}{d}\right)^{0.0998} \times \exp(-2.385 \ln(\frac{e}{d}))^2 \dots \dots \dots (16)$$

$$f = 366.46 Re^{-1.068} \left(\frac{x}{d}\right)^{0.6351} \exp(-0.1641 \ln(\frac{x}{d}))^2 \left(\frac{y}{d}\right)^{1.4643} \exp(0.2968 \ln(\frac{y}{d}))^2 \left(\frac{e}{d}\right)^{0.1047} \times \exp(-0.6009 \ln(\frac{e}{d}))^2 \dots \dots \dots (17)$$

Hence upon evaluating the comparison studies discussed above, it is clear that computational results are in good agreement with the experimental studies which justifies the credibility of the proposed numerical results in spherical dimpled channel.

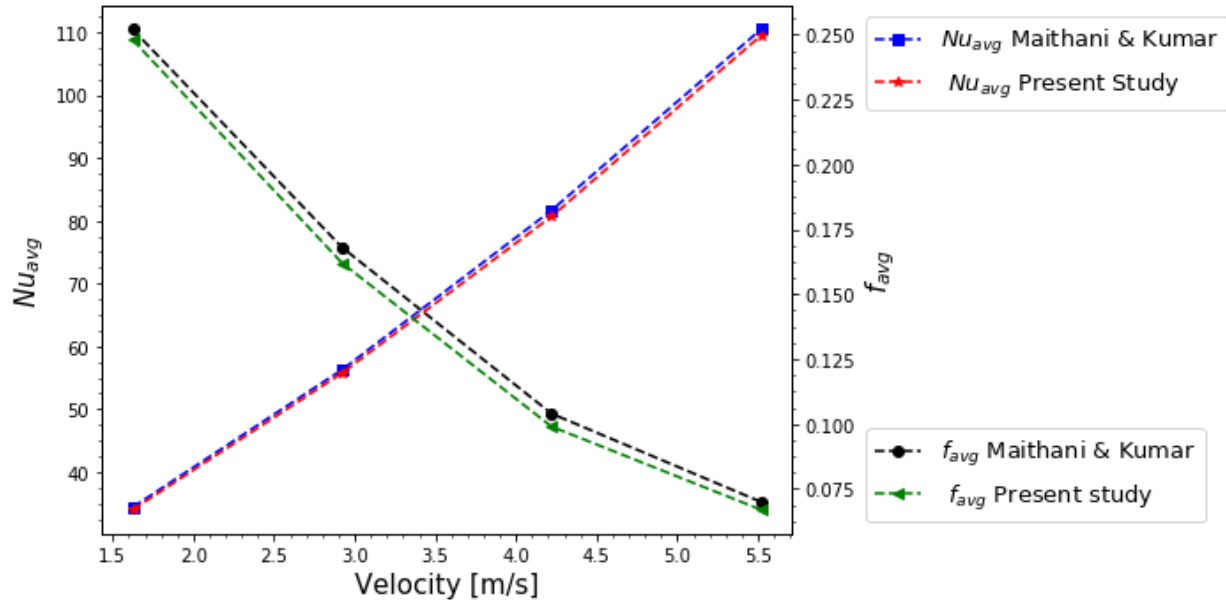


Figure 14: Comparison of Nu_{avg} and f_{avg} for dimpled Channel with traditional correlations

6. Results and Discussions

The present study primarily investigates and compares the thermal performance of dimpled channel with smooth channel using Soybean oil as coolant. Moreover, the study evaluates the performance of MXene (Ti_3C_2) nanofluid where Soybean oil is considered as base fluid. MXene nanofluid with 0.025%, 0.075% and 0.125% weight concentration were investigated in dimpled channel assuming single-phase approach. Both the laminar and turbulent flows were studied varying Reynolds number from 1000 to 6000.

6.1. Analysis of Velocity Distribution

Figure 15 shows the velocity distribution for base fluid, 0.025%, 0.075% and 0.125% weight concentrations of MXene nanofluid in dimpled channel at $Re\ 6 \times 10^3$. Due to having dimpled shapes, the secondary flow is induced near the dimpled surfaces [40]. As evaluated from contours, farther the flow streams move away from the dimpled wall, higher the velocity becomes. The maximum velocity was observed at the central region of the flow regime. The reason could be explained that apart from wall of the dimpled channel, the effect of boundary layer lessens. Hence the least effect of hydrodynamic boundary layer could be present at the central region of the channel which leads to reaching the maximum velocity at the center of the dimpled channel.

Though from the qualitative point of view, the velocity profiles are alike to each other, from the quantitative point of view, the magnitude of velocity for basefluid, 0.025%, 0.075% and 0.125% MXene nanofluid are different. The reasoning of variation in fluid velocity for basefluid, and nanofluids as shown in **Figure 15** are obvious due to having different buoyancy and viscous forces. In addition, the viscosity and density of the nanofluids are higher compared to basefluid which results in dynamic and thermal boundary layers to be thicker for nanofluids [45]. With the inclusion of MXene nanoparticles to the Soybean oil, the intermixing of the fluid layers is improved and induced secondary flow becomes more intense [45]. This phenomenon concludes that higher the inclusion of nanoparticles, larger the magnitude of velocity becomes. Therefore, the maximum velocity was evident for 0.125 wt% MXene, followed by 0.075 wt% MXene, followed by 0.025 wt% MXene, and minimum for Soybean oil. Moreover, the streamlines of the velocity fields were represented in the figure when it shows the direction of the tangential velocity components of the domain. The streamlines near the dimple illustrated the leeward and windward velocities near the dimpled shape.

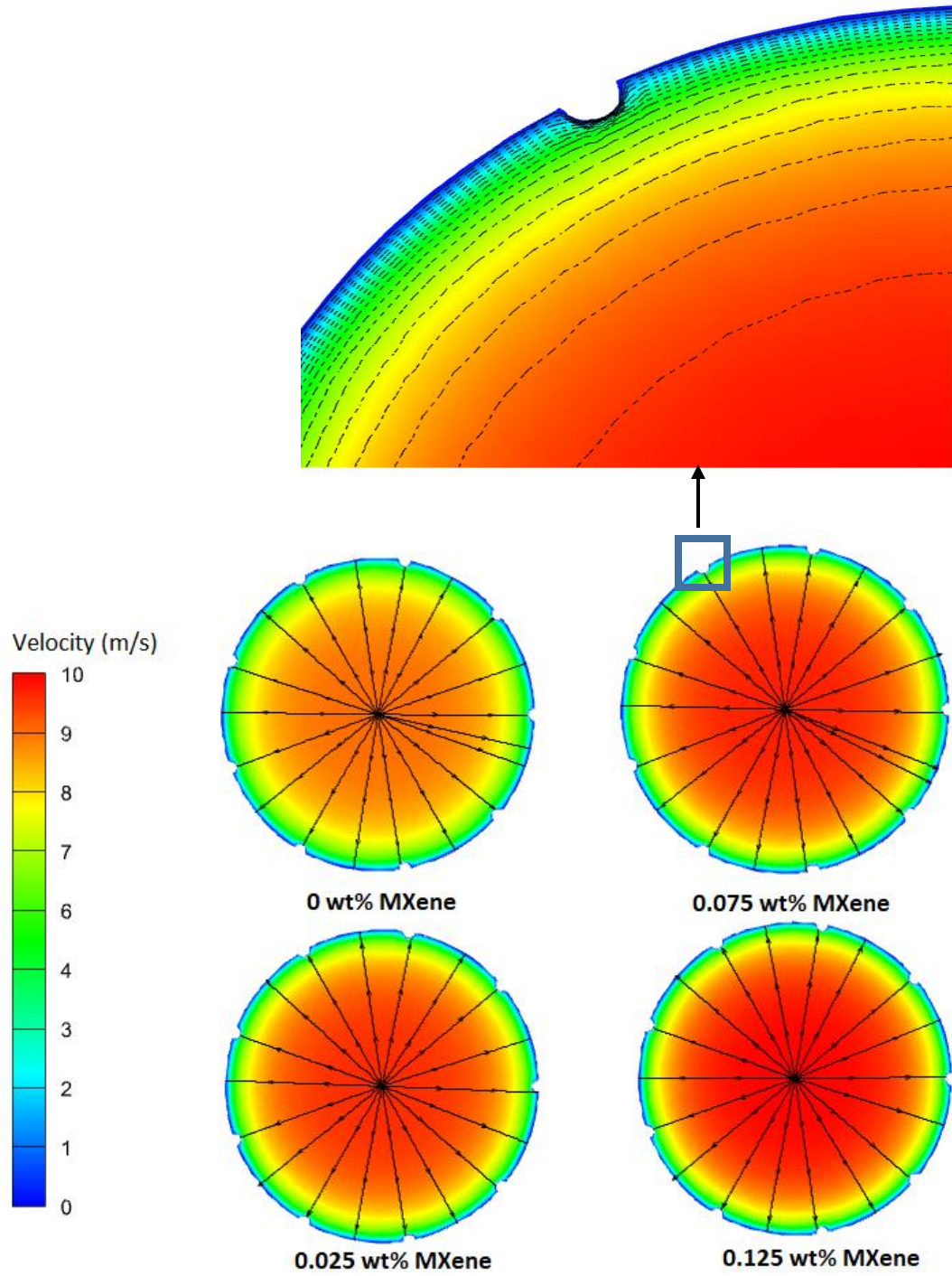


Figure 15: Comparison of Velocity Profiles at outlet of the flow regime for different thermofluids at Re 6000

Figure 16 shows the axial velocity profile for 0.125 wt% MXene at Re 6000. The windward and leeward velocity components were shown with the help of streamlines and velocity vectors. It is evident from the figure that windward velocity increases as it approaches to the upper side of the dimples and leeward velocity decreases as it reaches to the lower side of the dimple near the wall. Moreover, from the streamlines, the flow obstructions near the dimple is observed which essentially leads to the predominant behavior of turbulence near the dimpled walls.

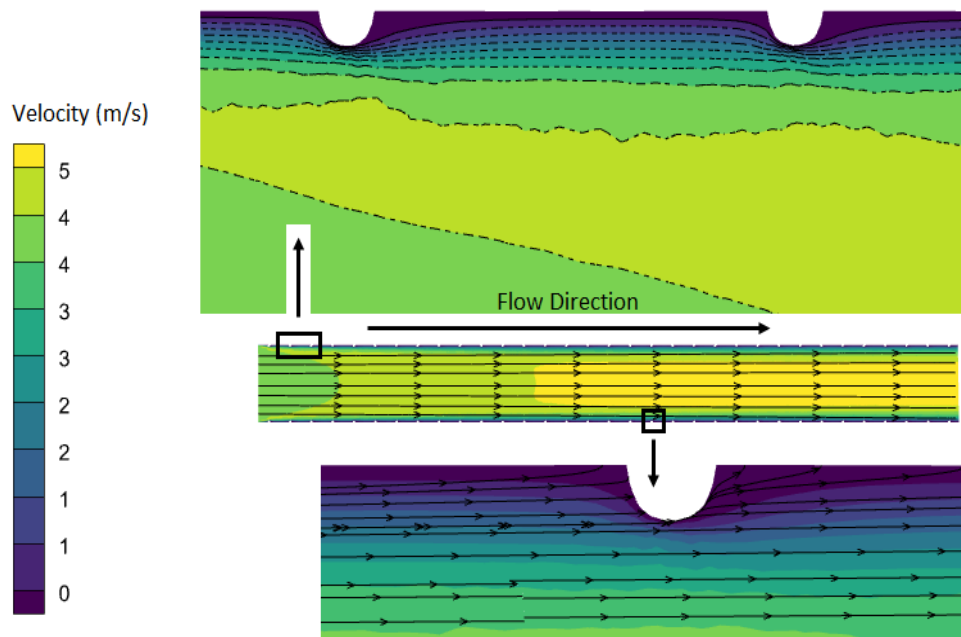


Figure 16: Representation of flow obstructions with streamlines and velocity vector near the dimpled zone for 0.125 wt% MXene at Re 6000

Figure 17 shows the velocity profile along the centerline of the axial flow regime for Soybean oil, 0.025, 0.075 and 0.125 wt% of MXene nanofluid at $Re\ 6 \times 10^3$. The identification could be made from the figure that inclusion of MXene nanoparticles have no significant contribution to velocity profile as the profiles found identical to each other. Since the mixture of nanoparticles to basefluid is assumed to be homogeneous mixture, the velocity of nanoparticles (V_{np}) and the velocity of basefluid (V_f) becomes

equal. Henceforward, the inclusion of nanoparticles does not affect the velocity profile significantly. Moreover, the observation could be made from **Figure 17** that, the hydrodynamic entrance length is around 0.50m at Re 6000, where the fully developed turbulent flow is achieved. In addition, it is well recognized that inclusion of nanoparticles does not affect the hydrodynamic entrance length of the fluid.

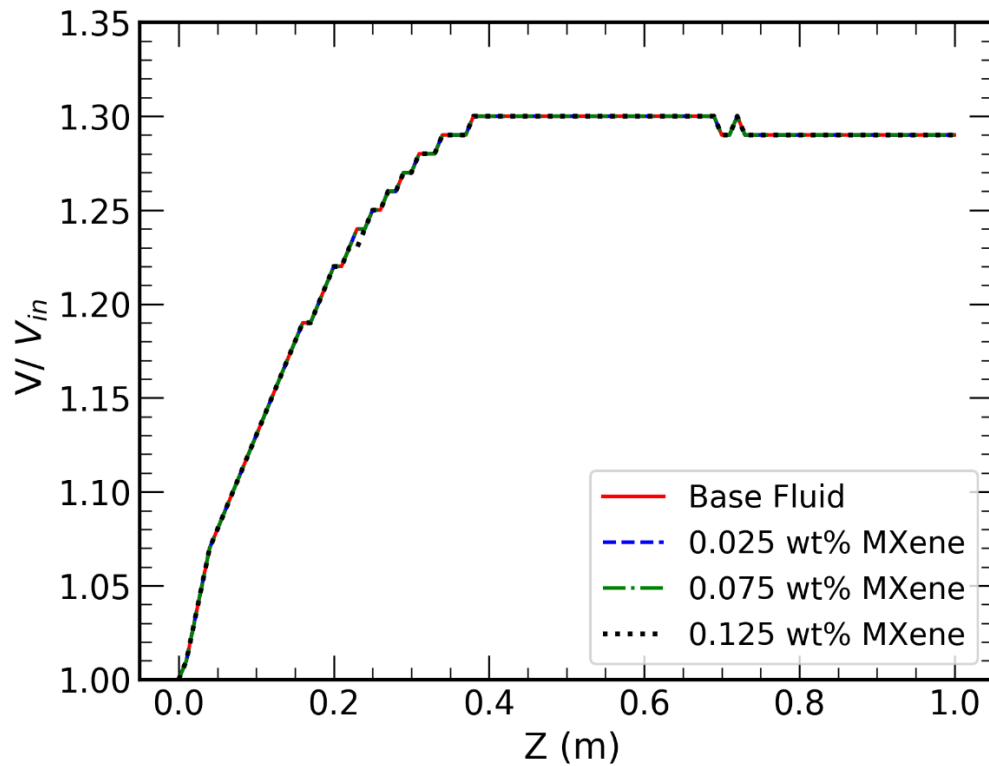


Figure 17: Development of Velocity Profiles at the centerline of the flow regime along axial direction for different thermofluids at Re 6000 in dimpled channel

6.2. Analysis of Turbulence Characteristics

Turbulence kinetic energy (TKE) plays a significant role to enhance the heat transfer. Hence the more the value of TKE, better the value of HTC becomes. **Figure 18** shows the development of TKE for basefluid, 0.025, 0.075 and 0.125 wt% MXene nanofluids at outlet of the flow regime for the value of $Re\ 6\times 10^3$. Due to having dimpled surfaces the value of TKE would be higher compared to smooth channel since dimple curves plays an important role to generate higher turbulence near wall region. Moreover, the value of TKE is found highest for 0.125 wt%, followed by 0.075 wt%, followed by 0.025 wt%, and least for basefluid as observed from **Figure 18**. The remarks could be drawn that inclusion of nanoparticles predominates the turbulence characteristics. Hence, with the upsurge in the weight concentration of nanofluids, the value of TKE increases. Additionally, as identified from **Figure 18**, the value of TKE for each cases were found highest near the wall, and gradually the value of TKE decreases apart from the wall of flow regime and least value of TKE was established at the central region of fluid domain.

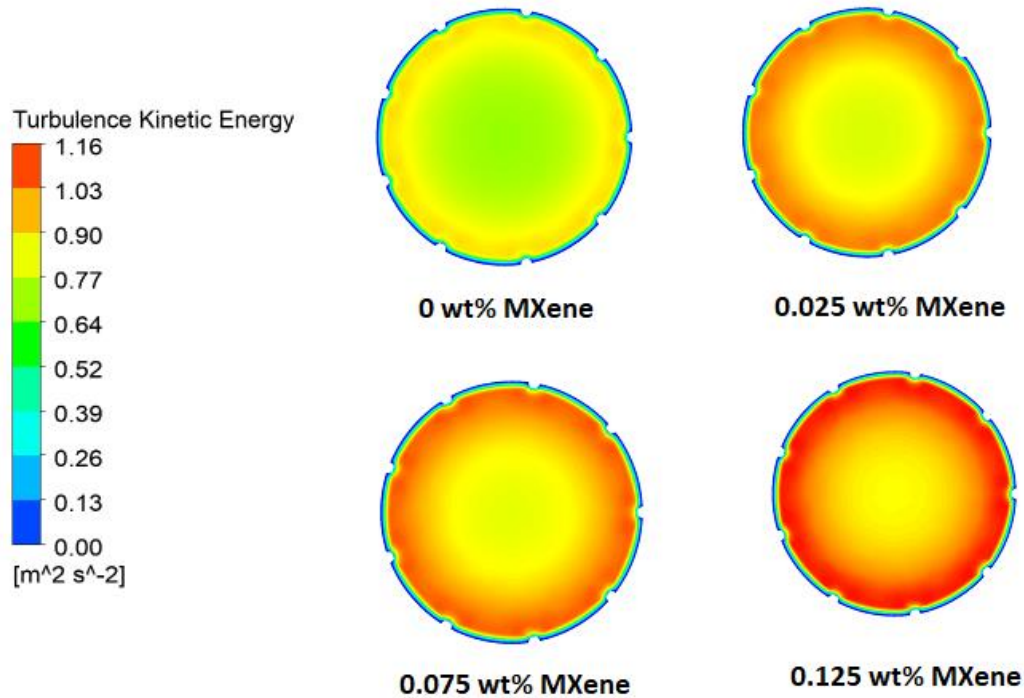


Figure 18: Comparison of TKE at outlet of the flow regime along radial direction for different thermofluids at $Re\ 6000$

6.3. Analysis of Temperature Distribution

Figure 19 shows the temperature distribution over the wall of the smooth channel and dimpled channel at $Re\ 6\times 10^3$. As observed in the figure, the wall temperature of the dimpled channel were found intensely lower compared to smooth channel. Dimpled surface played an important role to decrease the wall temperature through inducing secondary flow near the dimpled depths in the flow regime. Moreover, the growth of boundary layer gets interrupted due to dimpled surfaces which lead to increase in the turbulent intensity. The increased Turbulent Intensity (TI) predominantly enhanced the heat transfer and led to decrease in wall temperature. Additionally, the inclusion of MXene nanoparticles to base fluid lead to decrease in wall temperature even more compared to Soybean oil in the dimpled channel. Due to improvement in thermophysical properties of the coolant, the wall temperature of dimpled channel for 0.025 wt% is lower compared to base fluid, followed by 0.075 wt% and least for 0.125 wt%, as seen from the **Figure 19**.

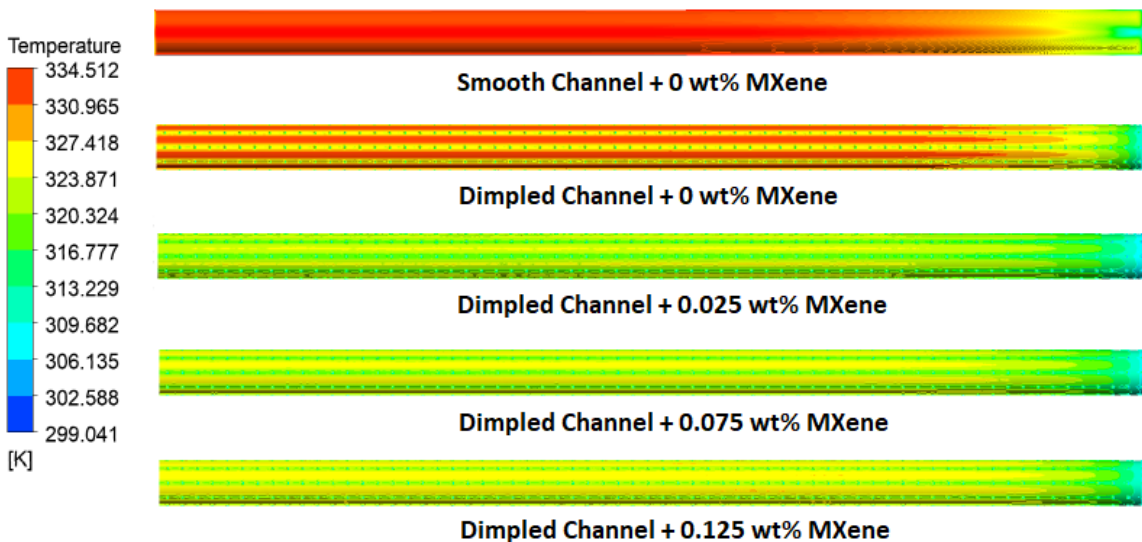


Figure 19: Comparison of temperature at the wall of flow regime along axial direction for different thermofluids at Re 6000

Figure 20 represented the temperature profile with isotherms over the wall of the dimpled channel at $Re\ 6000$. As observed from the figure, the multilayers of isotherms are generated near the dimple shapes of the channel. Along the direction of the flow, the temperature rises as the coolant gets hotter.

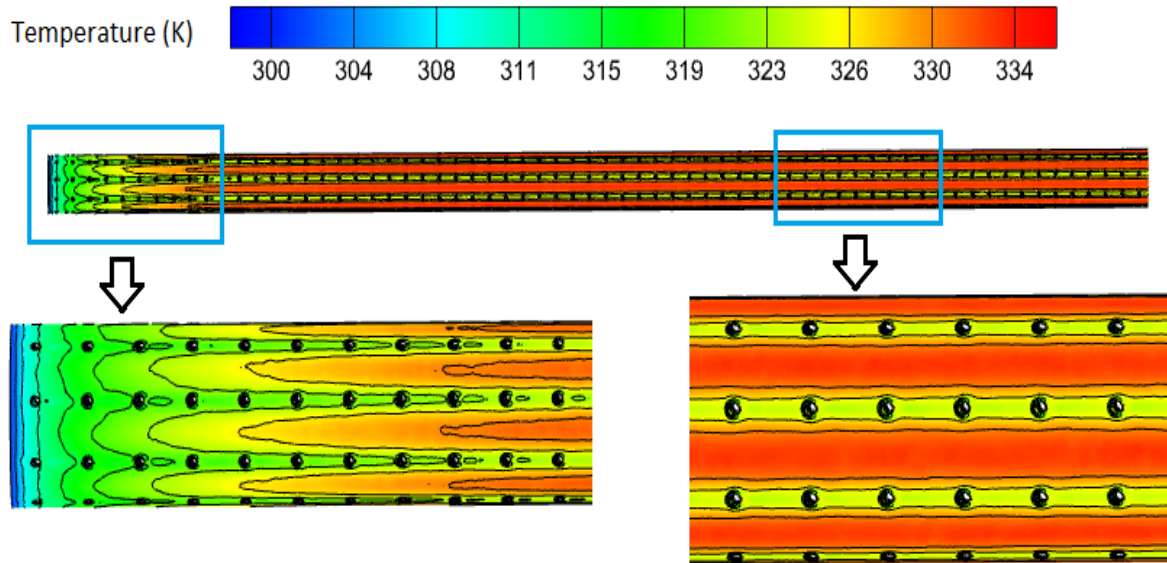


Figure 20: Representation of multi-layer isothermal lines and temperature profile for 0.125 wt% MXene at Re 6000

As stated by some researches [46][47][48], with the increase in volume concentration, the bulk temperature of the nanofluid will decrease. Such phenomenon is apparently visible in **Figure 21** which shows the centerline temperature of the dimpled channel at $Re\ 3 \times 10^3$. It is found in the figure that the centerline temperature is gradually increasing along the flow length and achieved highest for Soybean oil, followed by 0.025 wt%, followed by 0.075 wt%, and minimum value of centerline temperature was observed for 0.125 wt%.

Since constant heat flux was implemented to the channel wall, the magnitude of $\overline{T_w} - \overline{T_b}$ plays an essential role for the prediction of heat transfer coefficients (HTC) following Equation 10. It is identified from the **Figure 22** that with the increase in weight concentration as well as Re for both laminar and turbulent flow regime, the magnitude of $\overline{T_w} - \overline{T_b}$ seemed to be decreased. The maximum value of $\overline{T_w} - \overline{T_b}$ was observed for smooth channel with basefluid, which gradually decreased with the increase in weight concentration, and lowest value of $\overline{T_w} - \overline{T_b}$ was evaluated for dimpled channel with 0.125 wt%. However, numeric value of $\overline{T_w} - \overline{T_b}$ was identified higher in **Figure 22** for laminar ranged Re

compared to turbulent ranged Re which predicts that value of HTC will be eventually higher for turbulent flow compared to laminar flow.

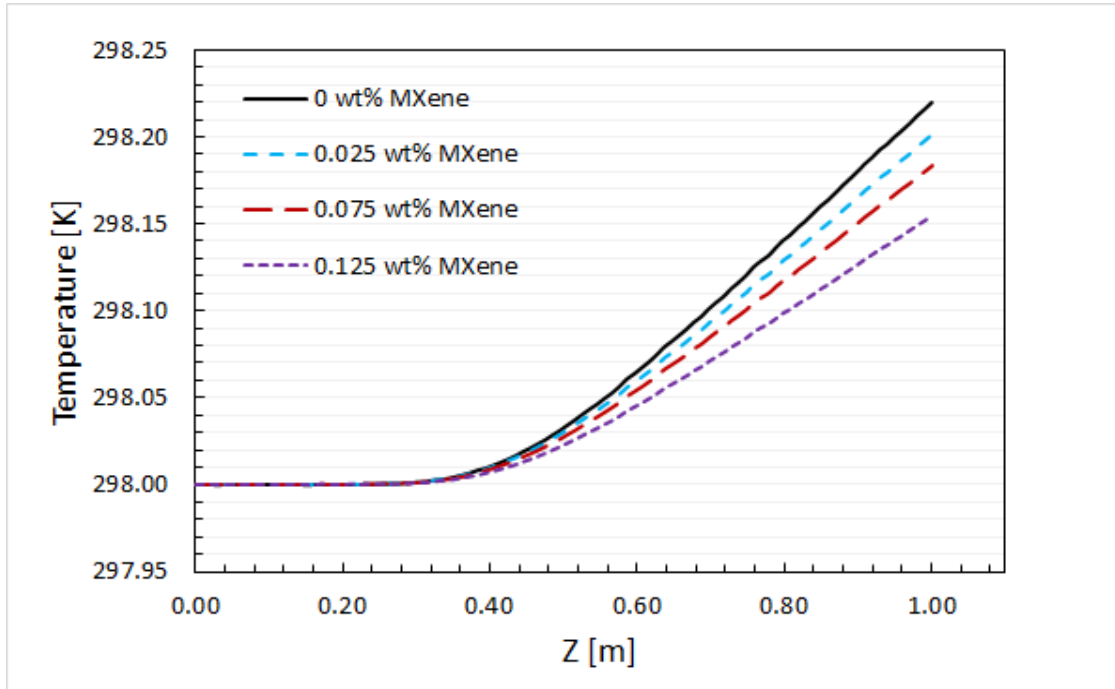


Figure 21: Comparison of temperature at the centerline of flow regime along axial direction for different thermofluids at Re 3000 in dimpled channel

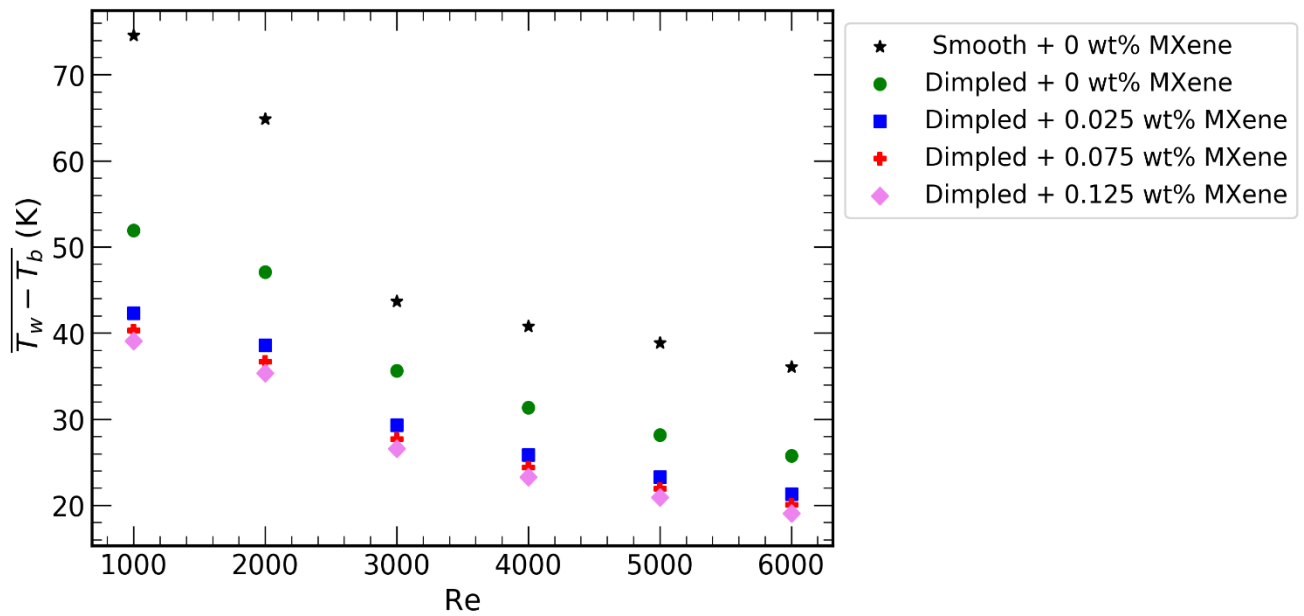


Figure 22: Variation in the magnitude of $\overline{T_w - T_b}$ with weight concentration for different value of Re

6.4 Analysis of Heat Transfer Coefficient (HTC) and Nusselt Number (Nu)

Inclusion of Nanoparticles to the basefluid improves the thermophysical properties of the nanofluids. Hence, Property Enhancement Ratio (PER) is a predominant factor to explain the enhancement of heat transfer while using nanofluid as coolant. Equation 18 represents the calculation of PER for nanofluids [49].

$$\text{Property Enhancement Ratio (PER)} = \frac{\text{Thermal Conductivity Improvement Ratio}}{\text{Viscosity Improvement Ratio}} \dots\dots\dots (18)$$

Where, $\text{Thermal Conductivity Improvement Ratio} = \frac{k_{nf}}{k_{bf}}$
 $\text{Viscosity Improvement Ratio} = \frac{\mu_{nf}}{\mu_{bf}}$

Table 1 represents the value of PER for different weight concentration of MXene nanofluid at inlet temperature.

Weight Concentration of Nanofluid	Property Enhancement Ratio (PER)
0.025 wt% MXene	1.084
0.075 wt% MXene	1.172
0.125 wt% MXene	1.233

Table 1: Representation of the value of PER for different weight concentrations of MXene nanofluids at inlet temperature

The value of averaged HTC was calculated following the Equation 10 and 11. **Figure 19** shows the variation of averaged HTC with varying Re for each investigated cases. As seen in the figure, the smooth channel with Soybean oil is having the lowest value of HTC compared to dimpled channel with Soybean oil as coolant. Additionally, for the cases of MXene nanofluids, it is evident from the figure that the value of averaged HTC is found highest for 0.125 wt%, followed by 0.075 wt%, followed by 0.025 wt%. The explanation of enhancement in heat transfer could be explained following the criteria of Property Enhancement Ratio (PER) as shown in Table 1. According to Table 1, the value of PER is least for 0.025 wt%, followed by 0.075 wt% and highest for 0.125 wt% of MXene nanofluid. The value of PER increased 8.4% for 0.025 wt%, 17.2% for 0.075 wt% and 23.3% for 0.125 wt% of MXene nanofluid

compared to Soybean oil. Due to having substantial improvement in the thermo-physical properties, the value of HTC was observed highest for 0.125 wt%, gradually decreases with the decrease in weight concentration and found lowest for basefluid.

In addition, the upsurge of heat transfer rate could be possible due to the effect of nanoparticles to the thickness of thermal boundary layer. The thickness of thermal boundary layers are decreased with the increase in the movement of nanoparticles within the fluid. This random movement within the fluid significantly upsurge the enhancement of heat transfer [50][51][52]. Therefore, inclusion of higher nanoparticles to the base fluid, will verily decrease the thermal boundary layer thickness even more, which will upsurge the heat transfer coefficient meaningfully.

Moreover, with the increase in the value of Re, the value of HTC is increased which is shown in **Figure 23**. Since with the increase in Re, the velocity of the coolant is increased, which eventually lead to the decrease in the value of $\overline{T_w - T_b}$. Therefore, supporting Equation 10, the value of HTC was observed to be increased with the increase in Re. The enhancement of, intermolecular forces, inertial forces and both probability and capacity of the fluid to obstruct separation were certainly increased with the increase in Re. This phenomenon leads to an upsurge in occurrences of fluid molecules to increase motion, which consequently leads to higher heat transfer [53].

Noted that, the increase in the value of HTC for turbulent ranged Re is quite high compared to laminar ranged Re. As discussed above, the value of $\overline{T_w - T_b}$ was found higher for laminar ranged Re compared turbulent ranges, following the Equation 10 and 11, the value of HTC will be lower for laminar ranged Re compared to turbulent ranges which is well identified in the **Figure 23**.

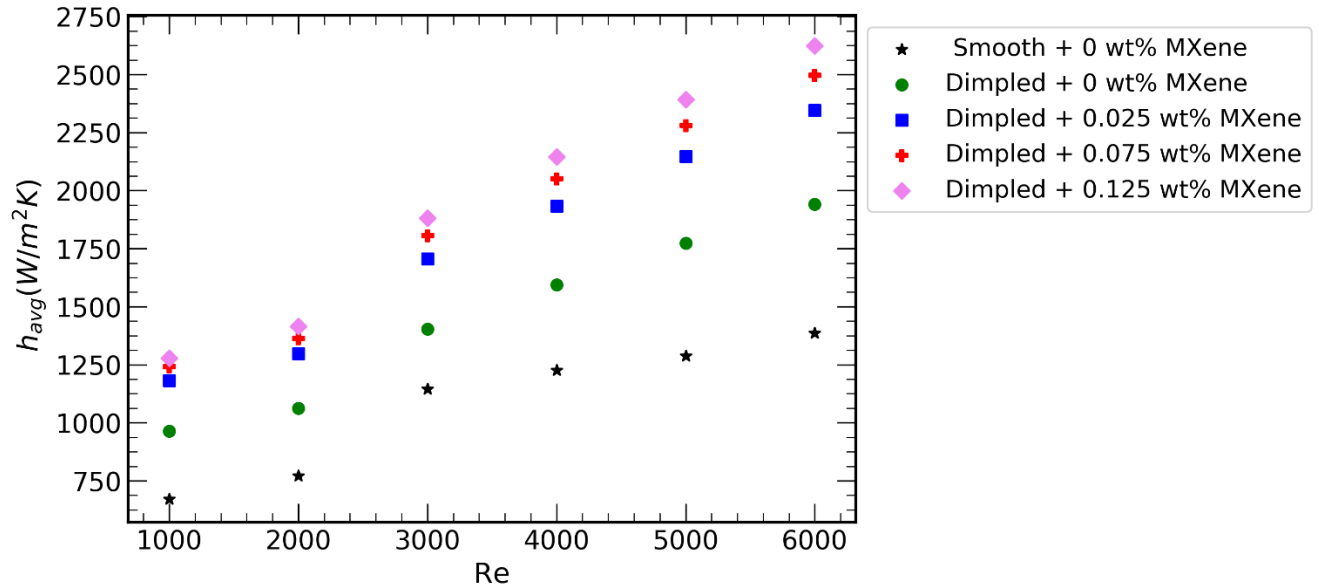


Figure 23: Variation of averaged heat transfer coefficient with Re for each investigated cases

Following Equation 12, the calculation of averaged Nu was carried out. **Figure 24** shows the variation of Nusselt number with Re for different investigated cases in the present study. The observation could be drawn from the figure that the highest value of Nu was evident for 0.125 wt %, which gradually decreases with the decrease in weight concentration, and the least value of Nu was observed for basefluid. Moreover, the value of Nu is increased with the increase in Re as seen in **Figure 24**.

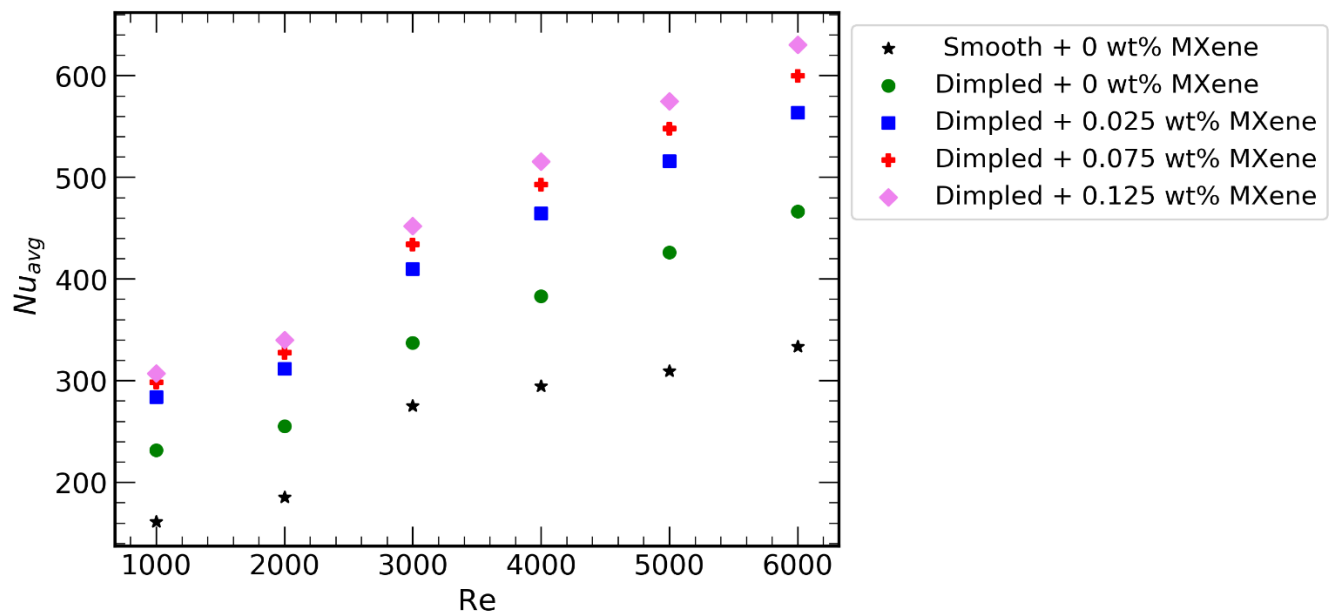


Figure 24: Variation of averaged Nusselt Number with Re for each investigated cases

6.5 Analysis of Pressure Drop

As discussed above, the inclusion of nanoparticles, improve the heat transfer coefficient of the coolant. However, the augmentation of nanoparticles leads to increased viscosity and density. Consequently, the increase in the cohesion of nanoparticles are evident during the fluid flow, which ultimately results in the upsurge of pressure drop [54]. **Figure 25** illustrates the variation of pressure drop along the centerline of axial flow direction in dimpled channel for 0 wt%, 0.025 wt%, 0.075 wt% and 0.125 wt% MXene nanofluid consecutively. The figure shows that along the axial direction of the coolant flow, the highest pressure drop was observed for 0.125 wt% MXene nanofluid, which gradually decreases with the decrease in weight concentration and become least for basefluid. Moreover, it is well recognized from the **Figure 25** that, along the direction of coolant flow, the pressure reduction follows linear trends

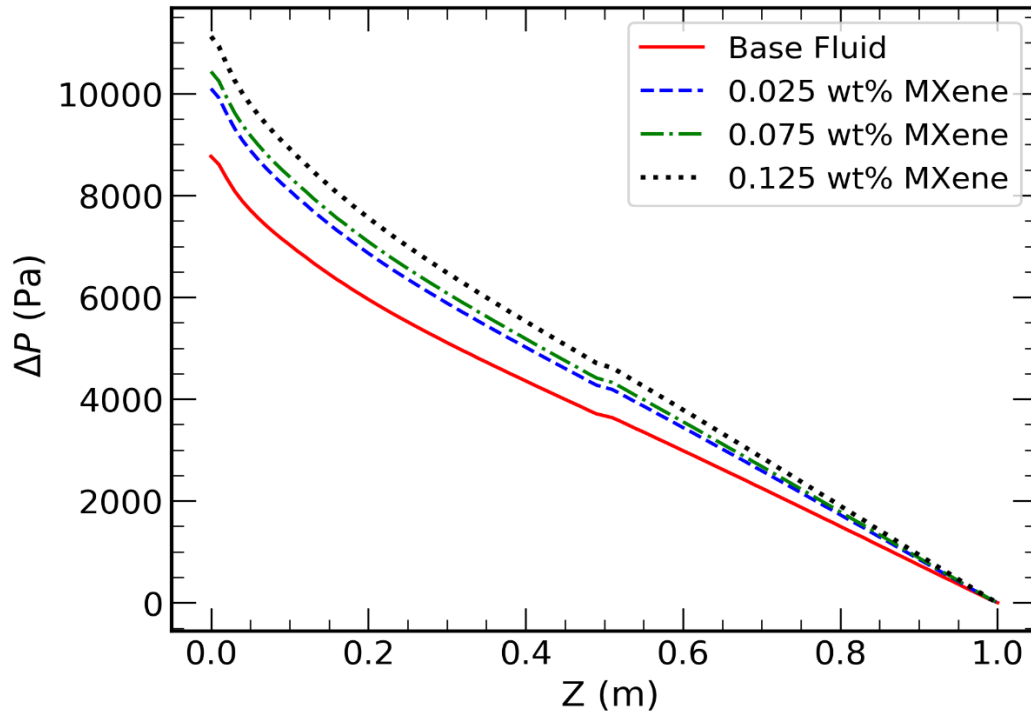


Figure 25: Variation of pressure drop along the centerline of the dimpled channel for different investigated cases at Re 3000

Figure 26 shows the averaged pressure drop for each investigated cases while varying Re. Noted that, compared to smooth channel, dimpled channel is exhibiting higher pressure drop due to blockades provided by the dimpled surfaces to the motion of the fluid. Furthermore, it is recognized from **Figure**

26 that the augmentation of nanoparticles increased the averaged pressure drop. Due to having higher cohesions between the nanoparticles, with the increase in weight concentration, the averaged pressure drop gradually increases. Hence maximum pressure drop was found for 0.125 wt%, which consecutively decreased and achieved least value for base fluid.

Moreover, as evident in **Figure 26**, the pressure drop increases with the increase in Re. Since, the increased in Re leads to an enhancement of hydrodynamic entrance length, which results in larger velocity gradient as well as higher shear stress near the wall region of entrance length. As a result, the pressure drop becomes higher at entrance region which leads to boost up the averaged pressure drop with the increase in Re [55].

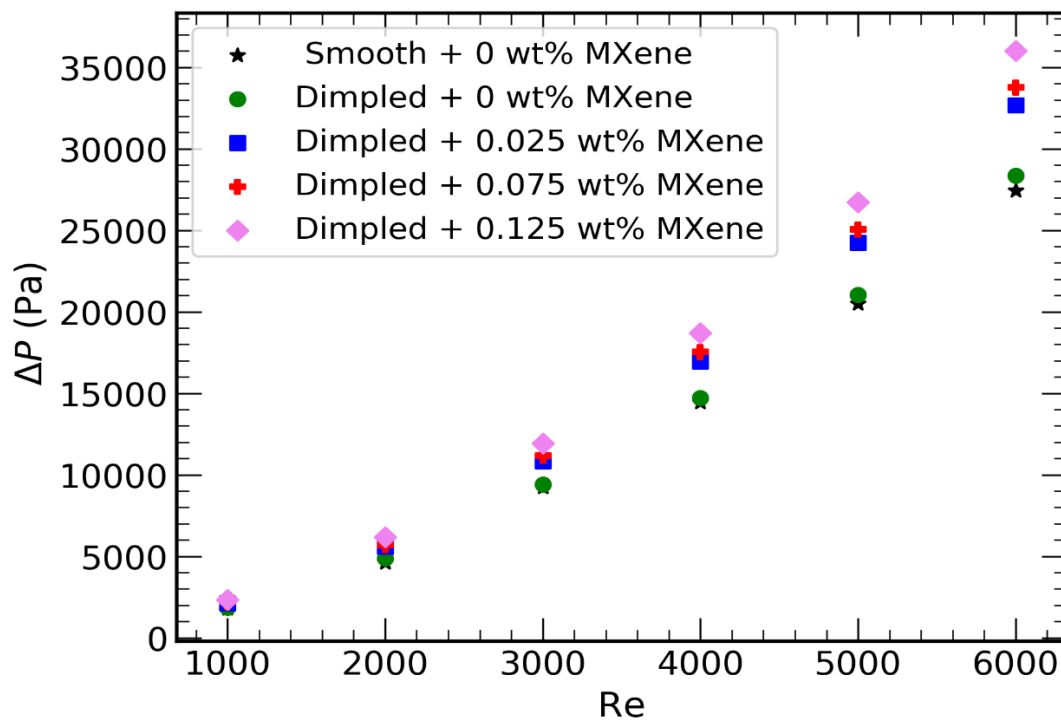


Figure 26: Variation of averaged pressure drop for each investigated cases with Re

The pumping power was evaluated following the Equation 19. **Figure 27** represents the pumping power as a function of Re. It is well understood that similar trends relevant to pressure drop would be evident for pumping power according to Equation 19. The highest pumping power was recognized for 0.125 wt%, which gradually decreases with the decreases in weight concentrations and the least value of pumping power is recognized for smooth channel. Moreover, noted that the pumping power was observed quite low for the laminar flow regime. The maximum value of 31.1% increase in pumping

power was observed for 0.125 wt% MXene which signifies the novelty of MXene/SO nanofluid due to having such lowered requirement of pumping power.

$$Pumping\ Power = \frac{\pi}{4} D_h^2 v \Delta P \dots\dots\dots (19)$$

Where, D_h stands for hydraulic diameter, v stands for velocity, and ΔP stands for averaged pressure drop

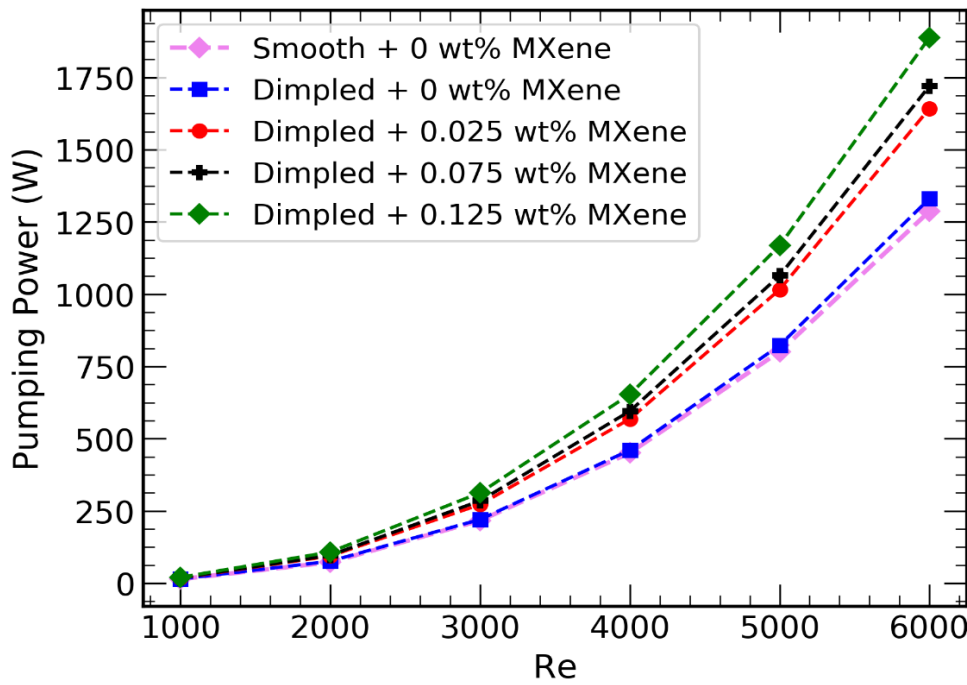


Figure 27: Variation of pumping power for each investigated cases with Re

6.6 Performance Analysis of Investigated Cases

As discussed above, the dimpled channel is showing higher heat transfer as well as pressure drop compared to smooth channel. Pressure drop is highly associated with pumping power and cost effectiveness since with the increase in pressure drop, requirement of pumping power increases. Hence to identify effectiveness of the geometry, thermal performance for rough surface was evaluated through Performance Evaluation Criterion ($PEC_{(rs)}$) as shown in Equation 20 [40][56]. PEC considers both the scenarios of enhancement in heat transfer and increase in pressure drop to provide thermal efficiency.

Moreover, alike with the scenario of rough surfaced dimpled channel, inclusion of nanoparticles enhances heat transfer coefficient with the cost of pressure drop. Consequently, in order to implement the nanofluid, the conclusion should be drawn considering both the enhancement of heat transfer as well as pressure drop. Hence thermal performance of nanofluid was evaluated following the similar approach to dimpled channel, using Performance Evaluation Criterion for nanofluids [41][44][56]. The computation of PEC for nanofluids is illustrated in Equation 21.

$$PEC_{(rs)} = \frac{Nu_{rs}/Nu_{ss}}{(f_{rs}/f_{ss})^{\frac{1}{3}}} \dots\dots\dots (20)$$

Where, Nu_{rs} and Nu_{ss} stand for Nusselt number for dimpled channel and smooth channels respectively. The friction coefficient for dimpled channel and smooth channel are illustrated using f_{rs} and f_{ss} respectively.

$$PEC_{(rs)} = \frac{Nu_{nf}/Nu_{bf}}{(f_{nf}/f_{bf})^{\frac{1}{3}}} \dots\dots\dots (21)$$

Where, Nu_{nf} and Nu_{bf} stand for Nusselt number for nanofluid and basefluid respectively. The friction coefficient for nanofluid and basefluid are illustrated using f_{nf} and f_{bf} respectively.

If the value of PEC is greater than unity, then it is obvious that heat transfer enhancement surpasses pressure loss. On the contrary, if the value of PEC is less than unity, it indicates that pressure loss surpasses heat transfer enhancement. **Figure 28** shows the thermal performance for each investigated cases with varying Re. As observed from the figure, it is recognized that the value of PEC for each cases of dimpled channel are greater than unity for both laminar and turbulent flow. Subsequently, it concludes that dimpled channel would be suitable compared to smooth channel as a heat exchanger considering the thermal performance. Compared to smooth channel, highest value of PEC for dimpled channel was observed at Re 1000, which is about 42.08%. However, the value of Re was seemed to be decreasing with the increase in Re up to laminar ranged Re. The reason might be that considerable amount of heat transfer is not noticeable to compensate the pressure loss for higher value of Re under laminar flow. On the contrary, the value of PEC was noticed increasing with the increase in Re and maximum 38.44% of increase in thermal performance was found at Re 6000.

The thermal performance of MXene nanofluids in the dimpled channel was found increased with the increase in weight concentrations. Henceforward, the maximum thermal performance was observed for 0.125 wt%, followed by 0.075 wt%, followed by 0.025 wt%, and lowest for basefluid. Maximum 88.9%

increase in thermal performance was observed for 0.125 wt% MXene, which is a remarkable improvement in terms of novelty of the investigated studies. Noted that, a maximum value of 83.22%, and 74.28% increase in thermal performance was observed for the cases of 0.075 wt%, and 0.025 wt% MXene nanofluid, which is also a noteworthy as well as noticeable improvement of thermal performances in terms of industrial application.

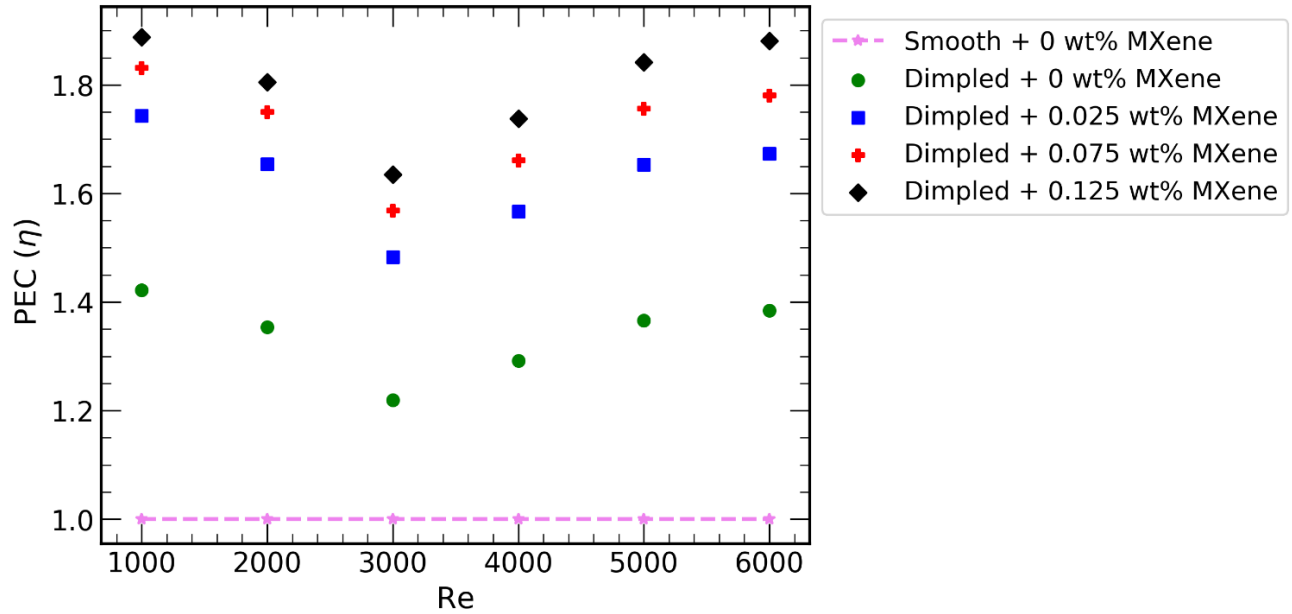


Figure 28: Variation of Performance Evaluation Criterion (PEC) for each investigated cases with Re

It is well evident from the discussion that, within the laminar flow regime, the value of PEC was decreased with the increase in Re. However, maximum value of PEC was identified at Re 1000 for each investigated cases of dimpled channel. On the contrary, the value of PEC was increasing with the increase in Re under turbulent flow regime, and achieved maximum value of PEC at Re 6000 for each investigated cases of dimpled channel. Hence the conclusion could be drawn from the discussion that the dimpled channel with basefluid as well as nanofluids will perform better at lower ranged Re under laminar flow regime. On the other hand, the dimpled channel with basefluid as well as nanofluid will exhibit higher thermal performances at higher value of Re under turbulent flow regime.

In order to evaluate the thermo-hydraulic performance of Silica based MXene nanoparticles, the present results were compared with the prominent study of Suresh et al.[17]. Suresh et al. [17] investigated the performance of helical arrangements of dimples with CuO-water nanofluid with 0.1%, 0.2% and 0.4%

concentrations. The study experimentally investigated the performance of CuO-water nanofluid under turbulent flow regime. Moreover, compared to the weight concentrations investigated in the study of Suresh et al. [17], it has to be noted that present study choose far lesser weight concentrations. **The experimental and numerical conditions of both the study were shown in Table 2. Figure 29** shows the comparison of the performance evaluation criterion (PEC) in between the present study and the experimental study of Suresh et al. [17]. The results indicated that with the increase in Re, the performance of the CuO-water nanofluid decreases haphazardly without following any trends.

Conditions	Present Study	Suresh et al. [17]
Flow Length	1000 mm	800 mm
Hydraulic Diameter	45 mm	4.85 mm
Channel	Dimpled	Dimpled
Nanoparticles	MXene	CuO
Weight Concentrations	0.025-0.125 wt%	0.1-0.3 wt%
Selected Re	1000-6000	2500 - 6000

Table 2: Study conditions of present investigation and Suresh et al. [17] investigation

As evident from the figure, present study supersedes the performance factor of CuO-water investigated by Suresh et al. large scaling factor. This justifies the credibility of MXene/SO nanofluid to be a novel coolant in the future for heat exchanger industries.

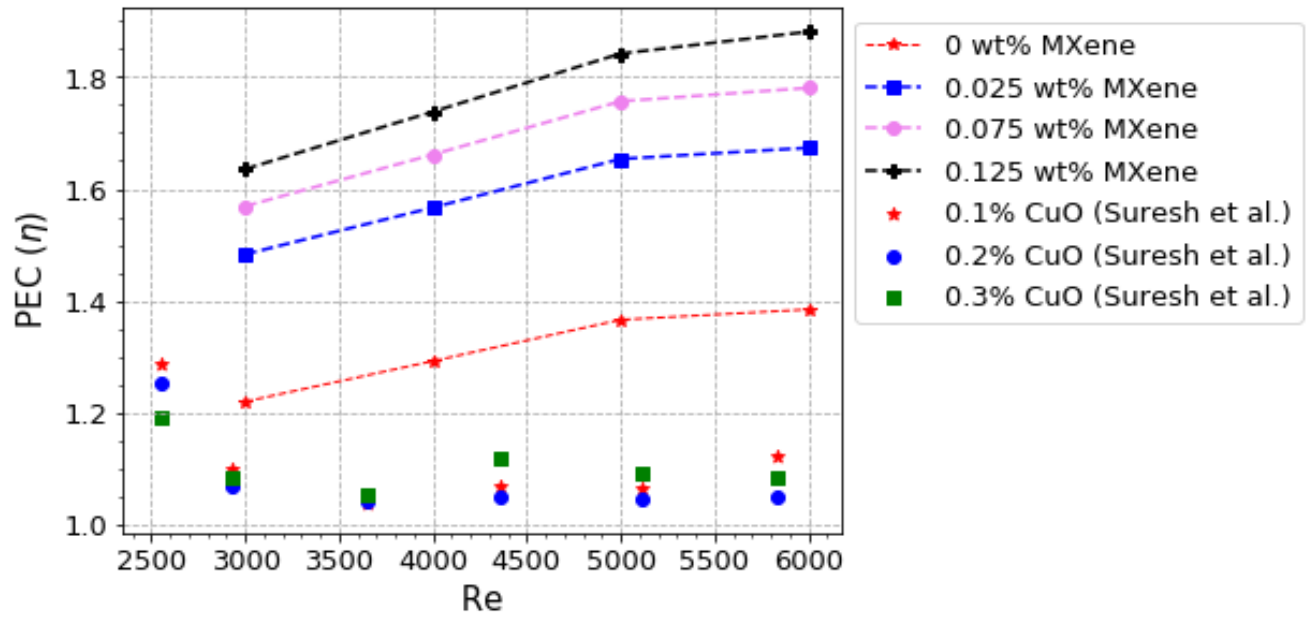


Figure 29: Comparison of Performance factor for different nanofluids in between the present study and the study of Suresh et al [17] in the dimpled channel

6.7 Discussion:

The study evaluated the performance of MXene/SO nanofluid in a dimpled channel for both the laminar and turbulent flow in order to justify the credibility in both the flow regime. A wide range of applications could be observed implementing dimple surface to enhance the thermal performance in compact heat exchangers, micro-heat exchangers, coaxial tube heat exchanger, and shell and tube heat exchanger [57]. Moreover, such surface roughness techniques could be applicable to micro and mini energy systems to cool down the systems with higher thermal performance such as cooling computer chips. Since such devices produce a huge amount of heat flux, an enhancement in cooling techniques such as dimpled surfaces could be appreciable [57]. Additionally, dimpled channel is also getting the focus on solar thermal energy conversion in absorber plate and tube due to its easy manufacturing, and not having any impact on the weight of the absorber. A compound technique that implement both the surface roughness and improvement of the coolant improves the thermal performance even more and reducing the global crisis of cooling. As discussed above, the credibility of MXene/SO nanofluid could be a potential coolant for the future studies with a wide range of applications. Though nanofluids were able to increase the thermal performance, due to higher inclusions of the nanoparticles, the industrial applications are getting

hindered. Nevertheless, higher inclusions of nanoparticles (about 1-5 wt %) improve the property of the coolant, it associates with major challenges such as clogging of nanoparticles, erosions of the pipelines specially due to metallic nanoparticles [18][58]. Moreover, addition of large number of nanoparticles would lead to larger pumping power which might affect the maintenance cost and higher kinetic and momentum energy that might damage the surface [59]. On the contrary, MXene nanoparticles investigated in the present study improved property enhancement ratio of the coolant up to about 23% with the inclusion of small amount of nanoparticles (0.125 wt %). As discussed above, the thermal performance of the nanofluid increases up to approximately 89% with the inclusion of 0.125 wt% MXene nanoparticles. Since, with the small inclusions of MXene nanoparticles, such a high thermal performance could be achievable, the major challenges depicted above could be mitigated with the help of MXene nanoparticles. Hence both the dimpled surfaces with MXene/SO nanofluid could be a potential solution to the cooling crisis in the field of the compact heat exchangers, micro/mini heat exchangers, solar thermal conversions, and micro/mini energy systems [60].

Conclusion:

In this research, the compound technique to improve the thermal efficiency was implemented which involves two passive methods, namely- Surface Roughness and improvement of coolant. Surface roughness was followed by spherical dimples over circular channel and improvement of coolant is associated with application of MXene/SO nanofluid, a new class and novel heat transfer fluid. The conclusions of the study are as follows:

- Compared to smooth channel, spherical dimpled channel shows incredibly higher thermal performance. A maximum increase of 42.15% thermal performance was observed due to application of dimpled surface roughness technique.
- With the inclusion of tiny amount of MXene nanoparticles, drastic improvement in thermophysical properties were achieved. A maximum increase of about 23.34% in the value of PER was achieved only with the inclusion of 0.125% MXene nanoparticles.
- With the increase in weight concentrations of MXene nanoparticles, heat transfer coefficient as well as pressure drop was increased. The highest enhancement in heat transfer coefficient was recognized to be 90.12% whereas the highest increase in pressure drop was recognized to be

31.1% for 0.125 wt% MXene nanofluid. Noted that, such a tremendous increase in heat transfer with the cost of lowered value of pressure drop indicates the authority of MXene/SO nanofluid as a novel heat transfer fluid.

- Taking into account with benefits of heat transfer rate to the penalty of pressure drop, thermal performance were evaluated where it shows that with the increase in weight concentration, the performance of the nanofluid increases. The maximum value of PEC was found 1.89 for 0.125 wt% with dimpled channel which increased approximately 89% thermal performance compared to traditional smooth channel.
- The value of PEC was observed to be decreasing with the increase in Re under laminar flow ranged Re, whereas the value of PEC was found to be increasing with the increase in Re under turbulent flow ranged Re. Hence, in order to implement MXene nanofluid with dimpled channel, the study suggests to take lowered Re under laminar flow conditions in order to achieve highest thermal performance.

Furthermore, the study developed curve fitted equations for thermophysical properties of Soybean Oil and MXene/SO nanofluids which will certainly help the researchers to implement such novel coolant in the relevant research field.

Nomenclature:

Abbreviation

CFD	Computational fluid dynamics
FVM	Finite Volume Method
TKE:	Turbulent Kinetic Energy
HTC:	Heat Transfer Coefficient
PEC:	Performance Evaluation Criterion
TI:	Turbulent Intensity
SO:	Soybean Oil
DPM:	Discrete Phase Method
PER:	Properties Enhancement Ratio

e/d: The ratio of dimple depth to dimpled diameter

x/d: Stream-wise spacing

y/d: Span-wise spacing

v: Velocity (m/s)

C_p : Specific heat of fluid (J/kg K)

D_h : Hydraulic diameter P pressure (N/m²)

q'' : Wall heat flux (W/m²)

T: Temperature (K)

Nu: Nusselt number

Pr: Prandtl number

Re: Reynolds number

wt%: Nanoparticle weight concentration in percentage

k: Thermal conductivity (W m⁻¹ K⁻¹)

W: Watt

Greek Letters

μ : Dynamic Viscosity ((N·s)/m²)

γ : Kinematic Viscosity (m²/s)

ρ : Density (kg/m³)

Subscripts

i, j, k tensor index

bf: Base fluid

nf: Nanofluid

b: Bulk

w: Wall

ref: Reference value

rs: Rough Surface

ss: Smooth Surface

np: Nanoparticle

avg: Averaged

0: Initial value

Z: Flow direction,

Velocity components u,

v, and w in x, y, and z

directions.

References:

- [1] Alzahrani, S. and Usman, S., 2019. CFD simulations of the effect of in-tube twisted tape design on heat transfer and pressure drop in natural circulation. *Thermal Science and Engineering Progress*, 11, pp.325-333.
- [2] Nalavade, S.P., Prabhune, C.L. and Sane, N.K., 2019. Effect of novel flow divider type turbulators on fluid flow and heat transfer. *Thermal Science and Engineering Progress*, 9, pp.322-331.
- [3] Ghachem, K., Aich, W. and Kolsi, L., 2021. Computational analysis of hybrid nanofluid enhanced heat transfer in cross flow micro heat exchanger with rectangular wavy channels. *Case Studies in Thermal Engineering*, 24, p.100822. Kaood, A. and Hassan, M.A., 2020. Thermo-hydraulic performance of nanofluids flow in various internally corrugated tubes. *Chemical Engineering and Processing-Process Intensification*, 154, p.108043.
- [4] Eiamsa-ard, S., Wongcharee, K., Kunnarak, K., Kumar, M. and Chuwattabakul, V., 2019. Heat transfer enhancement of TiO₂-water nanofluid flow in dimpled tube with twisted tape insert. *Heat and Mass Transfer*, 55(10), pp.2987-3001.
- [5] Ahmed, F., Abir, M.A., Redwan, A.S.M., Bhuiyan, A.A. and Mollah, A.S., 2021. The impact of D-shaped jaggedness on heat transfer enhancement technique using Al₂O₃ based nanoparticles. *International Journal of Thermofluids*, 10, p.100069.
- [6] Perwez, A., Shende, S. and Kumar, R., 2019. Heat transfer and friction factor characteristic of spherical and inclined teardrop dimple channel subjected to forced convection. *Experimental Heat Transfer*, 32(2), pp.159-178.
- [7] Chen, J., Müller-Steinhagen, H. and Duffy, G.G., 2001. Heat transfer enhancement in dimpled tubes. *Applied thermal engineering*, 21(5), pp.535-547.
- [8] Wang, Y., He, Y.L., Lei, Y.G. and Zhang, J., 2010. Heat transfer and hydrodynamics analysis of a novel dimpled tube. *Experimental thermal and fluid science*, 34(8), pp.1273-1281.
- [9] García, A., Solano, J.P., Vicente, P.G. and Viedma, A., 2012. The influence of artificial roughness shape on heat transfer enhancement: Corrugated tubes, dimpled tubes and wire coils. *Applied Thermal Engineering*, 35, pp.196-201.
- [10] Kumar, P., Kumar, A., Chamoli, S. and Kumar, M., 2016. Experimental investigation of heat transfer enhancement and fluid flow characteristics in a protruded surface heat exchanger tube. *Experimental Thermal and Fluid Science*, 71, pp.42-51.
- [11] Wen, D. and Ding, Y., 2004. Experimental investigation into convective heat transfer of nanofluids at the entrance region under laminar flow conditions. *International journal of heat and mass transfer*, 47(24), pp.5181-5188.

- [12] Xuan, Y. and Li, Q., 2003. Investigation on convective heat transfer and flow features of nanofluids. *J. Heat transfer*, 125(1), pp.151-155.
- [13] Maiga, S.E.B., Palm, S.J., Nguyen, C.T., Roy, G. and Galanis, N., 2005. Heat transfer enhancement by using nanofluids in forced convection flows. *International journal of heat and fluid flow*, 26(4), pp.530-546.
- [14] Gugulothu, R., Somanchi, N.S., Reddy, K.V.K. and Akkiraju, K., 2017. A review on enhancement of heat transfer in heat exchanger with different inserts. *Materials today: proceedings*, 4(2), pp.1045-1050.
- [15] Li, P., Zhang, D. and Xie, Y., 2014. Heat transfer and flow analysis of Al₂O₃–water nanofluids in microchannel with dimple and protrusion. *International Journal of Heat and Mass Transfer*, 73, pp.456-467.
- [16] Sinha, G.K. and Srivastava, A., 2017. Exploring the potential of nanofluids for heat transfer augmentation in dimpled compact channels: Non-intrusive measurements. *International Journal of Heat and Mass Transfer*, 108, pp.1140-1153.
- [17] Suresh, S., Chandrasekar, M. and Sekhar, S.C., 2011. Experimental studies on heat transfer and friction factor characteristics of CuO/water nanofluid under turbulent flow in a helically dimpled tube. *Experimental Thermal and Fluid Science*, 35(3), pp.542-549.
- [18] Suresh, S., Chandrasekar, M. and Selvakumar, P., 2012. Experimental studies on heat transfer and friction factor characteristics of CuO/water nanofluid under laminar flow in a helically dimpled tube. *Heat and Mass Transfer*, 48(4), pp.683-694.
- [19] Firoozi, A., Majidi, S. and Ameri, M., 2020. A numerical assessment on heat transfer and flow characteristics of nanofluid in tubes enhanced with a variety of dimple configurations. *Thermal Science and Engineering Progress*, 19, p.100578.
- [20] Zheng, L., Xie, Y. and Zhang, D., 2017. Numerical investigation on heat transfer performance and flow characteristics in circular tubes with dimpled twisted tapes using Al₂O₃-water nanofluid. *International Journal of Heat and Mass Transfer*, 111, pp.962-981.
- [21] Abdelrazik, A.S., Tan, K.H., Aslfattahi, N., Arifutzzaman, A., Saidur, R. and Al-Sulaiman, F.A., 2020. Optical, stability and energy performance of water-based MXene nanofluids in hybrid PV/thermal solar systems. *Solar Energy*, 204, pp.32-47.
- [22] Bakthavatchalam, B., Habib, K., Saidur, R., Aslfattahi, N., Yahya, S.M., Rashedi, A. and Khanam, T., 2021. Optimization of thermophysical and rheological properties of mxene ionanofluids for hybrid solar photovoltaic/thermal systems. *Nanomaterials*, 11(2), p.320.
- [23] Aslfattahi, N., Samyilingam, L., Abdelrazik, A.S., Arifutzzaman, A. and Saidur, R.J.S.E.M., 2020. MXene based new class of silicone oil nanofluids for the performance improvement of concentrated photovoltaic thermal collector. *Solar Energy Materials and Solar Cells*, 211, p.110526.

- [24] Kalbande, V.P., Walke, P.V. and Shelke, R., 2019. Aluminum-based thermal storage system with solar collector using nanofluid. *Energy Storage*, 1(6), p.e99.
- [25] Kalbande, V.P., Walke, P.V. and Rambhad, K., 2021. Performance of oil-based thermal storage system with parabolic trough solar collector using Al₂O₃ and soybean oil nanofluid. *International Journal of Energy Research*.
- [26] Xuan, Y. and Roetzel, W., 2000. Conceptions for heat transfer correlation of nanofluids. *International Journal of heat and Mass transfer*, 43(19), pp.3701-3707.
- [27] Lee, S., Choi, S.S., Li, S.A. and Eastman, J.A., 1999. Measuring thermal conductivity of fluids containing oxide nanoparticles.
- [28] Maliga, S.E.B., Palm, S.M., Nguyen, C.T., Roy, G. and Galanis, N., 2005. Heat transfer enhancement using nanofluid in forced convection flow. *Int. J. Heat fluid flow*, 26, pp.530-546.
- [29] Alhajaj, Z., Bayomy, A.M., Saghir, M.Z. and Rahman, M.M., 2020. Flow of nanofluid and hybrid fluid in porous channels: experimental and numerical approach. *International Journal of Thermofluids*, 1, p.100016.
- [30] Plant, R.D. and Saghir, M.Z., 2021. Numerical and experimental investigation of high concentration aqueous alumina nanofluids in a two and three channel heat exchanger. *International Journal of Thermofluids*, 9, p.100055.
- [31] Albojamal, A. and Vafai, K., 2017. Analysis of single phase, discrete and mixture models, in predicting nanofluid transport. *International Journal of Heat and Mass Transfer*, 114, pp.225-237.
- [32] Kim, D., Kwon, Y., Cho, Y., Li, C., Cheong, S., Hwang, Y., Lee, J., Hong, D. and Moon, S., 2009. Convective heat transfer characteristics of nanofluids under laminar and turbulent flow conditions. *Current Applied Physics*, 9(2), pp.e119-e123.
- [33] Wen, D. and Ding, Y., 2004. Experimental investigation into convective heat transfer of nanofluids at the entrance region under laminar flow conditions. *International journal of heat and mass transfer*, 47(24), pp.5181-5188.
- [34] Rubbi, F., Habib, K., Saidur, R., Aslfattahi, N., Yahya, S.M. and Das, L., 2020. Performance optimization of a hybrid PV/T solar system using Soybean oil/MXene nanofluids as A new class of heat transfer fluids. *Solar Energy*, 208, pp.124-138.
- [35] George H.F., Qureshi F., 2013. Newton's Law of Viscosity, Newtonian and Non-Newtonian Fluids. In: Wang Q.J., Chung YW. (eds) *Encyclopedia of Tribology*. Springer, Boston, MA. https://doi.org/10.1007/978-0-387-92897-5_143
- [36] Aghanajafi, A., Toghraie, D. and Mehmandoust, B., 2017. Numerical simulation of laminar forced convection of water-CuO nanofluid inside a triangular duct. *Physica E: Low-Dimensional Systems and Nanostructures*, 85, pp.103-108.

- [37] Ahmed, F., Abir, M.A., Bhowmik, P.K., Deshpande, V., Mollah, A.S., Kumar, D. and Alam, S., 2021. Computational assessment of thermo-hydraulic performance of Al₂O₃-water nanofluid in hexagonal rod-bundles subchannel. *Progress in Nuclear Energy*, 135, p.103700.
- [38] Ghazanfari, V., Talebi, M., Khorsandi, J. and Abdolahi, R., 2016. Thermal–hydraulic modeling of water/Al₂O₃ nanofluid as the coolant in annular fuels for a typical VVER-1000 core. *Progress in Nuclear Energy*, 87, pp.67-73.
- [39] Velagapudi, V., Konijeti, K.R. and Aduru, K.S.C., 2008. Empirical correlations to predict thermophysical and heat transfer characteristics of nanofluids. *Thermal Science*, 12(2), pp.27-37.
- [40] Kumar, A., Maithani, R. and Suri, A.R.S., 2017. Numerical and experimental investigation of enhancement of heat transfer in dimpled rib heat exchanger tube. *Heat and Mass Transfer*, 53(12), pp.3501-3516.
- [41] Ahmed, F., Abir, M.A., Bhowmik, P.K., Deshpande, V. and Mollah, A.S., 2021. Thermohydraulic performance of water mixed Al₂O₃, TiO₂ or graphene-oxide nanoparticles for nuclear fuel triangular subchannel. *Thermal Science and Engineering Progress*, p.100929.
- [42] Fluent Inc. (2006) Fluent 6.3 User's Guide 2006. Fluent Inc., Lebanon.
- [43] Dittus, F.W. and Boelter, L.M.K., 1985. Heat transfer in automobile radiators of the tubular type. *International communications in heat and mass transfer*, 12(1), pp.3-22.
- [44] Maithani, R. and Kumar, A., 2020. Correlations development for Nusselt number and friction factor in a dimpled surface heat exchanger tube. *Experimental Heat Transfer*, 33(2), pp.101-122.
- [45] Benkhedda, M., Boufendi, T. and Touahri, S., 2018. Laminar mixed convective heat transfer enhancement by using Ag-TiO₂-water hybrid Nanofluid in a heated horizontal annulus. *Heat and Mass Transfer*, 54(9), pp.2799-2814.
- [46] Bianco, V., Manca, O. and Nardini, S., 2011. Numerical investigation on nanofluids turbulent convection heat transfer inside a circular tube. *International Journal of Thermal Sciences*, 50(3), pp.341-349.
- [47] Bianco, V., Chiacchio, F., Manca, O. and Nardini, S., 2009. Numerical investigation of nanofluids forced convection in circular tubes. *Applied Thermal Engineering*, 29(17-18), pp.3632-3642.
- [48] Hussien, A.A., Yusop, N.M., Moh'd A, A.N., Abdullah, M.Z., Janvekar, A.A. and Elnaggar, M.H., 2019. Numerical study of heat transfer enhancement using Al₂O₃-graphene/water hybrid nanofluid flow in mini tubes. *Iranian Journal of Science and Technology, Transactions A: Science*, 43(4), pp.1989-2000.
- [49] Ahmed, F., Abir, M.A., Fuad, M., Akter, F., Bhowmik, P.K., Alam, S. and Kumar, D., 2021. Numerical investigation of the thermo-hydraulic performance of water-based nanofluids in a dimpled channel flow using Al₂O₃, CuO, and hybrid Al₂O₃-CuO as nanoparticles. *Heat Transfer*.

- [50] Osman, S., Sharifpur, M. and Meyer, J.P., 2019. Experimental investigation of convection heat transfer in the transition flow regime of aluminium oxide-water nanofluids in a rectangular channel. *International Journal of Heat and Mass Transfer*, 133, pp.895-902.
- [51] Kim, D., Kwon, Y., Cho, Y., Li, C., Cheong, S., Hwang, Y., Lee, J., Hong, D. and Moon, S., 2009. Convective heat transfer characteristics of nanofluids under laminar and turbulent flow conditions. *Current Applied Physics*, 9(2), pp.e119-e123.
- [52] Duangthongsuk, W. and Wongwises, S., 2010. An experimental study on the heat transfer performance and pressure drop of TiO₂-water nanofluids flowing under a turbulent flow regime. *International Journal of Heat and Mass Transfer*, 53(1-3), pp.334-344.
- [53] Zarringhalam, M., Karimipour, A. and Toghraie, D., 2016. Experimental study of the effect of solid volume fraction and Reynolds number on heat transfer coefficient and pressure drop of CuO–water nanofluid. *Experimental Thermal and Fluid Science*, 76, pp.342-351.
- [54] Abdollahi-Moghaddam, M., Motahari, K. and Rezaei, A., 2018. Performance characteristics of low concentrations of CuO/water nanofluids flowing through horizontal tube for energy efficiency purposes; an experimental study and ANN modeling. *Journal of Molecular Liquids*, 271, pp.342-352.
- [55] Gupta, S., Sharma, A., Singh, K. and Srivastava, K.K., 2013. Hydrodynamic and thermal study of water in narrow copper tube. *Indian Chemical Engineer*, 55(4), pp.294-306.
- [56] Lewis, M.J., 1975. Optimising the thermohydraulic performance of rough surfaces. *International Journal of Heat and Mass transfer*, 18(11), pp.1243-1248.
- [57] Rashidi, S., Hormozi, F., Sundén, B. and Mahian, O., 2019. Energy saving in thermal energy systems using dimpled surface technology—A review on mechanisms and applications. *Applied Energy*, 250, pp.1491-1547.
- [58] Mahian, O., Kolsi, L., Amani, M., Estellé, P., Ahmadi, G., Kleinstreuer, C., Marshall, J.S., Siavashi, M., Taylor, R.A., Niazmand, H. and Wongwises, S., 2019. Recent advances in modeling and simulation of nanofluid flows-Part I: Fundamentals and theory. *Physics reports*, 790, pp.1-48.
- [59] Mahian, O., Kolsi, L., Amani, M., Estellé, P., Ahmadi, G., Kleinstreuer, C., Marshall, J.S., Taylor, R.A., Abu-Nada, E., Rashidi, S. and Niazmand, H., 2019. Recent advances in modeling and simulation of nanofluid flows-part II: applications. vol. 791. *Phys Rep*, pp.1-59.
- [60] Ben Said, L., Kolsi, L., Ghachem, K., Almeshaal, M. and Maatki, C., 2021. Advancement of nanofluids in automotive applications during the last few years—a comprehensive review. *Journal of Thermal Analysis and Calorimetry*, pp.1-28.